Calcareous nannofossils across the Eocene-Oligocene transition at Site 756 (Ninetyeast Ridge, Indian Ocean): implications for biostratigraphy and paleoceanographic clues

Allyson Viganò[1*], Helen K. Coxall[2], Max Holmström[2], Martina Vinco[1], Caroline H. Lear [3], Claudia Agnini[1]

Authors' addresses

[1]Dipartimento di Geoscienze, Università di Padova, Via Gradenigo 6 – 35131, Padova, Italy;

email: allyson.vigano@phd.unipd.it, claudia.agnini@unipd.it

[2]Department of Geological Sciences, Stockholm University, SE-106 91 Stockholm, Sweden;

email: helen.coxall@geo.su.se

[3]School of Earth and Environmental Sciences, Cardiff University, Main building, Park Place, Cardiff CF10 3AT, UK;

email: learc@cardiff.ac.uk

* corresponding author: allyson.vigano@phd.unipd.it

Abstract. The timing and modalities of calcareous phytoplankton community and evolutionary responses to the Eocene-Oligocene transition (EOT, ~ 34 Ma) are still under-investigated. In order to better constrain the dynamics of these pelagic primary producers during the climate transition, we conducted high resolution assemblage analysis on calcareous nannofossils across a ~19 m-thick interval of nannofossil ooze at Ocean Drilling Program (ODP) Site 756 (Ninetyeast Ridge, Indian Ocean; Peirce et al. 1989) (paleolatitude ~43°S; Zachos et al. 1992). We explored the diversity patterns against a new integrated planktonic foraminifera and calcareous nannofossil biostratigraphy produced for the site, as well as new benthic foraminifera stable isotope (C, O) record, which documents ocean-climate changes, and provides independent chemostratigraphy. The study section spans nannofossil Zones NP20-NP23 (equivalent to CNE20-CNO4) and lasts 5.6 Myr. The results show that the hankeninid extinction falls within the ~4.5 m-thick EOT isotopic interval (0.67 m below the base of the second positive $\delta^{18}O$ shift - EOIS), which is consistent with previous studies, making Hole 756C one of a few sites globally boasting both the familiar stepped $\delta^{18}O$ and $\delta^{13}C$ structure of the EOT and the primary biostratigraphic marker defining the base of the Oligocene. A series of potentially useful new calcareous nannofossil bioevents were identified that could help improve dating and correlation of this crucial interval. In this context, changes in calcareous nannofossil assemblages observed across EOT are interpreted in terms of modifications of paleoecological parameters that typically control the abundance and distribution of different taxa. Variations in sea surface temperature and nutrient availability are considered to be the most likely triggers for the calcareous phytoplankton changes observed across EOT. Specifically, our data suggest

that increased nutrients in the mixed layer played a key role in shaping the late Eocene - early Oligocene calcareous nannofossil assemblages.

Keywords: calcareous nannofossils, biostratigraphy, paleoecology, Eocene-Oligocene transition, ODP Hole 756C.

1 Introduction

The Eocene-Oligocene transition denotes a period of profound change during the Cenozoic and coincides with the onset of a permanent ice cap on Antarctica (e.g., Coxall and Pearson 2007, Hutchinson et al. 2021). The transition from a largely ice-free greenhouse world (Eocene) to an icehouse climate (Oligocene) characterized by a major glaciation on the South Pole and global cooling (e.g., Zachos et al. 2001) is documented by diverse geological evidence from around the world including glacio-marine deposits, sea water cooling, ice growth, sea-level fall, calcite compensation depth (CCD) deepening and important extinction and turnover in the marine biota (Pälike et al. 2006, 2012, Coxall and Pearson 2007, Pearson et al. 2008, Lear et al. 2008, Coxall and Wilson 2011, Hutchinson et al. 2021). During this time, the marine ecosystem suffered a variety of abrupt modifications - e.g., major turnovers were observed in radiolarians and diatoms (Baldauf 1992, Funakawa et al. 2006, Moore et al. 2014), planktonic foraminifera (Diester-Haass and Zahn 2001, Pearson et al. 2008, Wade and Pearson 2008, Wade and Olsson 2009) and calcareous nannofossils (Dunkley Jones et al. 2008, Bordiga et al. 2015, Jones et al. 2019), dramatic extinctions have been documented in large benthic foraminifera (Cotton and Pearson 2011), diverse proxies recorded variations in the global carbon cycling, productivity (Coxall and Pearson 2007) and silica supply (Egan et al. 2013, Fontorbe et al. 2017).

The possible triggers for the EOT are still vigorously debated and include different mechanisms: (1) the opening of the southern oceanic gateways, the Drake Passage and the Tasman Gateway, which led to the initiation of the Antarctic Circumpolar current (ACC) and the thermal isolation of Antarctica (Kennett 1977), (2) a long-term decrease in atmospheric pCO_2 (DeConto and Pollard 2003) associated with an eccentricity minimum and low-amplitude obliquity, promoted cooler summers – preventing ice, accumulated during the winter season, from melting (Coxall et al. 2005), or (3) a combination of the two (e.g., Drake Passage opening resulting in reduced pCO_2), as recently suggested by Lear and Lunt (2016).

Strong evidence for ice expansion comes from a two-stepped positive shift documented in benthic (1.5‰) and planktonic (~1‰) foraminiferal oxygen stable isotopes ($\delta^{18}O$) (Coxall et al. 2005, Coxall and Wilson 2011).

Following the terminology recently proposed by Hutchinson et al. (2021), these two steps are here referred to as "Step 1" and "EOIS", and all together constitute the EOT, which is bounded at the base by the extinction of calcareous nannofossil *Discoaster saipanensis*. The Eocene-Oligocene boundary (EOB) appears to fall in the plateau between the two isotopic steps, although only a limited number of studies have sufficiently well preserved planktonic foraminifera records and benthic foraminifera $\delta^{18}O$ and $\delta^{13}C$ to document this pattern and none, thus far, from the pelagic Indian Ocean (Coxall and Pearson 2007, Dunkley Jones et al. 2008, Pearson et al. 2008, Coxall and Wilson 2011, Hutchinson et al. 2021). The phase following the EOT and characterized by maximum $\delta^{18}O$ values, is here denoted as the 'Early Oligocene Glacial Maximum' (EOGM; Liu et al. 2004, Hutchinson et al., 2021).

It is commonly accepted that the changes in $\delta^{18}O$, observed during the Eocene-Oligocene transition, reflect variations both in ice-volume and sea water temperature (Zachos et al. 2001). In order to quantify the contribution of ice-volume signal from $\delta^{18}O$ record, Lear et al. (2008) published a $\delta^{18}O$-independent SST record from Tanzania using planktonic Mg/Ca paleothermometry. According to this study, the initial planktonic $\delta^{18}O$ step (Step 1) coincides with a decrease in Mg/Ca value (equivalent to ~2.5 °C cooling), recently corroborated by Bohaty et al. (2012), instead the second $\delta^{18}O$ step (EOIS) primarily reflects the expansion of the Antarctic cryosphere.

The stepwise pattern documented in $\delta^{18}O$ seems to be associated, with a 10 kyr lag, to a perturbation in the benthic and planktonic foraminiferal $\delta^{13}C$ records. The positive excursion in $\delta^{13}C$, as well as the deepening of the CCD, have been proposed to be related to increased sea surface productivity and consequent enhanced global burial of organic carbon in the deep sea, which would have caused an abnormally high storage of ^{12}C in the sediments (Zachos et al. 1996, Salamy and Zachos 1999, Zachos and Kump 2005, Coxall et al. 2005, 2018, 2021, Merico et al. 2008, Ravizza and Paquay 2008, Coxall and Wilson 2011, Bordiga et al. 2015, Armstrong Mckay et al. 2016, Jones et al. 2019, López-Quirós et al. 2021).

More recently, a shelf-to-basin shift in marine carbonate deposition in response to the sea level fall has been hypothesized as an additional mechanism behind the shift in $\delta^{13}C$ toward more positive values (Merico et al. 2008, Pälike et al. 2012) coupled to the sequestration of ^{12}C-enriched carbon into carbon capacitors (e.g., permafrost and marine methane hydrates) and possibly increased ocean ventilation (Armstrong Mckay et al. 2016).

A commonly held opinion is that the greenhouse-to-icehouse transition might have coincided with the onset of Arctic-imprinted North Component Water (NCW) mass, the ancient precursor of the North Atlantic Deep Water (NADW), which in turn probably impacted the poleward heat transport in both hemispheres (Davies et al. 2001, Via and Thomas 2006, Abelson and Erez 2017, Coxall et al. 2018). Changes in thermohaline circulation are fundamental to understand the evolution of climate because they are at the base of complicated balances and fluxes between deep waters as well as upper and mixed ocean layers.

Among the marine plankton, planktonic foraminifera were deeply affected during this time and suffered several extinctions. Wade and Pearson (2008) reported the abrupt extinction of all five remaining planktonic foraminifera species of the family Hantkeninidae, which formally defines the Eocene-Oligocene boundary (EOB; Premoli Silva and Jenkins 1993). The extinction of *Hantkenina* has been associated with a period of profound climate instability and increased nutrients in the photic zone (Pearson et al. 2008).

Like planktonic foraminifera, calcareous nannoplankton experienced a major turnover and a distinct shift toward less diverse assemblages rather than dramatic extinctions at the boundary.

To date, calcareous nannofossil responses still lack a global perspective and only few high-resolution studies are available for the EOT at high (Southern Ocean; Persico and Villa 2004, Villa et al. 2008, 2014) and mid-low latitudes (Tanzania, Dunkley Jones et al. 2008; South Atlantic, Bordiga et al. 2015; Equatorial Indian Ocean, Fioroni et al. 2015, Villa et al. 2021; Indonesia, Jones et al. 2019). From a biostratigraphic point of view, the E-O transition is characterized by a low rate of evolution, despite assemblage compositional changes, which is reflected in a scarcity of useful calcareous nannofossils biohorizons (Raffi et al. 2016). In some cases, the ranking and spacing of some bioevents, but also their quality and reliability, are still ambiguous and need to be further evaluated (Agnini et al. 2014). From a paleoecological perspective, the environmental pressure seems to have triggered important changes in the relative abundance of calcareous nannofossil species/taxa, diversity index, community structure and ecology. The present work focuses on three main goals: (1) to document ocean, climate and biotic responses in the eastern Indian Ocean at high-resolution across the Eocene-Oligocene transition at Site 756 (ODP Leg 121), (2) to potentially refine the number and position of calcareous nannofossil bioevents during this crucial time for future correlations over wide areas, (3) to provide a paleoecological interpretation based on abundance variations and distributions of calcareous nannofossil genera in order to reconstruct the characteristics of the sea surface waters in terms of temperature and productivity.

2 Material and methods

2.1 ODP Site 756

Sediments documenting the Eocene-Oligocene transition (EOT) were retrieved in the eastern Indian Ocean during ODP Leg 121 (Peirce et al. 1989). ODP Site 756 is the southern end member of a north-south paleoceanographic transect of seven sites drilled on Broken Ridge and Ninetyeast Ridge. At this site, a 227 m-thick section was drilled at four holes (A-D) and spans from the upper Eocene through Pleistocene.

The drilling was terminated after penetrating 82 m of volcanic basalt in Hole 756D (Peirce et al. 1989b).

The lithostratigraphic units (reported as meter below seafloor, mbsf) comprises: Subunit IA (0-144.5 m; nannofossils and foraminifera ooze), Subunit IB (144.5-150.3 m; foraminifera limestone) and Unit II (150.3-221.0 m; composed of vesicular basalts) (Peirce et al. 1989). Importantly, the drilled Paleogene carbonate ooze sequence contains a continuous sequence across the Eocene-Oligocene boundary, and is thus suitable to carry out detailed studies. Many other open-ocean E/O sequences are either incomplete or poorly preserved (Hutchinson et al., 2021 and references therein). In this study we analyzed samples from Hole 756C, which is located at 27°21.25'S, 87°35.89'E, in a water depth of 1516 m, near the crest of Ninetyeast Ridge (Fig. 1).

The investigated material belongs to the Subunit IA (0-144.5 m) and consists of a white nannofossil ooze with foraminiferal content varying between 5% and 20%. Trace amounts of radiolarians, sponge spicules, and silicoflagellates occur throughout the ooze (Peirce et al. 1989). The samples analyzed span from 113.46 to 132.70 mbsf, with an average spacing of ~20 cm and a temporal resolution of ca. 55 kyr.

2.2 Geological setting and Indian Ocean paleoceanography

During the Eocene, the Ninetyeast Ridge, today situated at a lower bathyal depth and bathed by Indian Central Water (Sverdrup et al. 1942), is inferred to have been influenced by several water masses operating simultaneously: the Indian Deep Water (IDW), the warm low-latitude Tethyan-Indian saline water (TISW, likely originating from the Tethyan or northern Indian Ocean) probably very similar in character to present day intermediate waters from the Arabian and Red seas, and possibly by other cold high latitude water masses, i.e., the Antarctic Intermediate Water (AAIW) and Antarctic Bottom Water (AABW) (Zachos et al. 1992).

ODP Site 756 has an estimated paleodepth of ~400 m (Zachos et al. 1992) and was likely bathed by the TISW.

146 The reconstructed paleolatitude indicate a significantly further South position (~43°S) during the Eocene
147 relative to the present day (~7°S) (Zachos et al. 1992). During the study interval, this site thus represents an
148 intermediate biogeographic domain located between low-middle and high latitudes (Fig. 1).
149 At the onset of the Oligocene, the two shallow-intermediate water-masses (TISW and AAIW) were still
150 flowing in the Indian Ocean, that are thought to have experienced a significant cooling related to the early
151 Oligocene onset of Antarctica ice-cap expansion. During the EOT, the cool AABW was likely reinforced by a
152 more vigorous circulation promoted by the onset of Antarctica, and eventually lead to the upwelling of nutrient
153 rich waters (Zachos et al. 1996) and to a further cooling (~2-3°) of deep-surface (thermocline) waters (Bohaty
154 et al. 2012). Moreover, the location of this site on a southeastern slope with irregular topography might have
155 favored the direct upwelling of these deeper water masses (Nomura 1991).
156
157 **2.3 Calcareous nannofossil data**
158 Counts on the calcareous nannofossil assemblages have been carried out on a total of 102 samples, prepared
159 using standard smear slide technique (Bown and Young 1998). Smear slides were analyzed using a Zeiss
160 optical microscope, at 1250× magnification, in cross-polarized (XPL) and phase-contrast (PC) light.
161 Calcareous nannofossils were identified to species/genus level, depending on coccolith preservation.
162 For instance, the overgrowth of *Discoaster* and the etching of *Chiasmolithus* in some cases prevent the
163 identification at species level. With few exceptions, the taxonomy adopted is that of Aubry (1984, 1988, 1989),
164 Perch-Nielsen (1985), Bown (2005), Bown and Dunkley Jones (2012) and Bown and Newsam (2017).
165 In particular, in accordance with Romein (1969), we ascribe *formosa* to genus *Ericsonia* (Agnini et al. 2014).
166 We also separate genus *Dictyococcites* from genus *Reticulofenestra* to maintain these genera as distinct
167 taxonomic units (Agnini et al. 2014, Fornaciari et al. 2010, Perch-Nielsen 1985).
168 We define *Reticulofenestra umbilicus* using the morphometric definition of Backman and Hermelin (1986),
169 which includes specimens >14μm. Relative abundance (%) data (Dataset S1) have been collected for species
170 and genera based on counts of at least 300 specimens per sample (Pospichal 1991). Semi-quantitative
171 abundance of selected taxa (Dataset S2) was determined by counting the number of specimens in a prefixed
172 area (n/mm^2; Backman and Shackleton 1983). This method allows to catch in detail the occurrence of selected
173 taxa, even those showing a sporadic occurrence (Agnini et al. 2014). The position of biostratigraphic and

isotopic tie-points were compiled to construct an age-depth model for Hole 756C and calculate LSRs, based on the Geological Time Scale 2012 (GTS12; Gradstein et al. 2012).

Principal component analysis (PCA), based on the correlation matrix (Q-mode; variables normalized with respect to variance), was performed on a set of relative abundance data, for a total of 13 taxa (Dataset S3), using the statistical software Past (Paleontological Statistic; Hammer et al. 2001).

PCA is a descriptive and explorative method that allows us to reduce the species variability in the dataset to a few number of factors (components) that allow a two-dimensional representation of the samples assemblage composition variability (Hammer and Harper 2006). This approach facilitates the visualization of our data, helping us to detect the major 'loading' genera and to investigate the main environmental factors affecting changes on calcareous nannofossil assemblage. Shannon's index (H) was used to quantify the diversity of nannoplankton for each sample, with low values indicating lower species richness and high values corresponding to dominance assemblages (Shannon and Weaver 1949).

Microphotos of markers species, as well as several calcareous nannofossil taxa, are provided (Pl. 1, 2, 3).

2.4 Foraminifera sample preparation and planktonic foraminifera biostratigraphic analysis

A total of 122 x 20 cc sand-fraction samples were prepared for foraminifera analysis. Bulk sediment samples were first disaggregated in deionized water on a shaker table at 175 rpm for at least one hour. The suspended sample was then poured onto a 63µm mesh sieve and washed with deionized water to separate the sand size particles. The >63µm residues were dried in an oven at 50 °C overnight before being transferred to labelled glass vials for storage.

Planktonic foraminiferal biostratigraphy was based on assemblage-counts performed on a subset of fifty-three of the samples. Here we focus on documentation of the position of relevant EOT biostratigraphic markers only, especially species of *Hantkenina*, *Globigerinatheka, Pseudohastigerina* and *Turborotalia*. Full planktonic foraminiferal assemblage counts are not reported here. Assemblages were examined using a Zeiss binocular stereo light microscope. Taxonomic determinations follow Pearson et al. (2006) and Wade et al. (2018).

Counts were based on the standard 300-specimen approach. Samples were first reduced to a split containing several hundred whole planktonic foraminifera specimens using a microsplitter (Shaw 1964). For the counting, each split sample was randomly strewn on a picking tray with a numbered grid (squares from 1 to 45). In order to reach the 300-specimen target, a random number generator was used to select grid squares. The order

generated was followed until approximately 300 planktonic foraminifera specimens had been counted. This was repeated for both the >180 µm and 63 µm fractions. For the extinction of *Hantkenina*, which denotes the E/O boundary (Premoli Silva and Jenkins 1993), additional (non-quantitative) scouring of the whole samples was performed to pin-down the event (>180µm and 63 µm fractions). Selected planktonic and benthic foraminifera were imaged using the scanning electron microscopes (SEM) at the Department of Geological Sciences (IGV), Stockholm University to document important taxa and test preservation states (Pl. 4).

2.5 Geochemical analyses

Bulk stable isotope data and $CaCO_3$ content. Bulk carbon and oxygen stable isotopes ($\delta^{13}C$ and $\delta^{18}O$) and calcium carbonate content (% $CaCO_3$) (Dataset S4) were analyzed using a Thermo Scientific Delta V Advantage spectrometer equipped with a Gas Bench II device at the Department of Geosciences (University of Padova). A known mass of sample (~0.30 mg) was weighed using the precision balance Mettler Toledo AT21 and placed into vials, subsequently flushed with helium. Each sample was then treated with 10 ml of orthophosphoric acid (EMSURE ® ≥ 99 %) for ca. 3 hours before the mass spectrometer analysis. Isotopic values are reported in standard delta notation relative to the Vienna Pee Dee Belemnite (VPDB). Raw $\delta^{13}C$ and $\delta^{18}O$ values were normalized through an internal standard (white Carrara marble Maq1: $\delta^{13}C$ = 2.58‰; $\delta^{18}O$= −1.15‰VPDB) periodically calibrated to NBS-19 IAEA reference material (Coplen et al. 2006).
For quality assurance, we used another internal standard, named as marble Gr1 ($\delta^{13}C$ = 0.68‰; $\delta^{18}O$= −10.44‰ VPDB). The CO_2 beam height (mV), which is a function of the carbonate content of the sample (Spofforth et al. 2010), was obtained during the mass spectrometer analysis. To calculate the carbonate content of each sample, a ramp of at least 10 samples of Maq1 (with weights ranging from 0.050 to 0.500 mg) was distributed along the run, and used to construct a linear fit (with R^2= 0.99).

Benthic foraminifera stable C and O isotopes. Benthic foraminifera were picked from the 250-500 µm fraction of the sand-sized sample set (see above for sample preparation). 122 monospecific samples were prepared, comprising the epifaunal species *Cibicidoides mundulus* or *Cibicidoides havanensis.*
The *C. mundulus* and *C. havanensis* sample sets were generated at different times (2014 and 2015 respectively); *C. havanensis* is more consistently present in the upper part of the studied section. Comparison of the data for the different species shows minimal differences, thus we present an integrated species record

(Dataset S5) for our EOT chemostratigraphy. Benthic foraminifera taxonomy followed Morkhoven et al. (1986) and Nomura et al. (1991). Test preservation was determined as moderate to well-preserved.

For each sample, 2-3 specimens were analysed to provide a target weight of 0.1-0.3 mg $CaCO_3$, as determined by the detection limits of the mass spectrometer. Sample weights were determined using a Sartorius MC5 microbalance (0.001 mg resolution). Benthic $\delta^{13}C$ and $\delta^{18}O$ was measured at Stockholm University using a Thermo Scientific MAT252 mass spectrometer attached to a GasBench II flow preparation and inlet system. An offline preparation step involved first drying the samples in an oven at 50° to remove any excess water before flushing the vials with helium. Each sample was reacted with 100 µl of 99% phosphoric acid before introduction to the mass spectrometer. Isotopic values were calibrated against the international standard VPDB. The reproducibility was determined to be 0.07‰ for $\delta^{13}C$ and 0.15‰ for $\delta^{18}O$.

3 Results

3.1 Biostratigraphy

Abundance patterns of index calcareous nannofossil species obtained from semi-quantitative counts (Fig. 3) were used to biostratigraphically frame the succession with reference to the biohorizons proposed in standard (Martini 1971, Okada and Bukry 1980) and additional biozonations (Agnini et al. 2014) (Fig. 2).

Biohorizons have been labelled according to published Cenozoic calcareous nannofossil biozonations (Backman et al. 2012, Agnini et al. 2014, Raffi et al. 2016) as follows: Base (B; stratigraphic lowest occurrence of a taxon), Top (T; stratigraphic highest occurrence of a taxon), Base common and continuous (Bc) and Top common and continuous (Tc), respectively the lowest and highest common and continuous occurrence of a taxon.

At Hole 756C, three planktonic foraminifera bioevents were recognized: the Top (T) of *Globigerinatheka index*, the Top of *Hantkenina* (comprising *H. alabamensis* and *H. primitva*), and the Top of large (>180µm) *Pseudohastigerina* (Table 1). In particular, we find the Top of *G. index* at 126.8 mbsf. It is recorded again in a sample 2 meters above this level (124.80 mbsf) (Dataset S6). However, the preservation is poor here and it is possible that this is reworked or a misidentified dentoglobigerinid, which can look rather similar. We therefore take the lower level for the Top of *G. index* event. It is also noted that there is a shift to a *'Dentoglobigerina taci'*-type assemblage above this horizon. Hantkeninids, belonging to the species *H. alabamensis* and *H. primitva* only, are not common at Site 756 (<1%). However, they are extremely distinctive,

and biostratigraphically critical thus worth hunting down. The highest occurrence of *Hantkenina* in our count data is at 125.0 mbsf. More detailed scouring of the whole samples around this horizon, including in the >63 µm fraction where sometimes broken tubulospines are the only remaining trace, pinned the Top *Hantkenina* spp. event down to 124.50 mbsf.

Pseudohastigerina micra and *P. naguewichiensis* are also rare (Pl. 4. Figs. 15-20) but persistent throughout the section. Significantly, at 127.0 mbsf, *Pseudohastigerina* no longer occurs in the >180 µm fraction but continues in the >63 µm fraction (Dataset S6). This we interpret as the '*Pseudohastigerina* dwarfing' event recognized previously (Nocchi et al. 1986, Wade and Pearson 2008). We are unable to place the *Turborotalita cerroazulensis-cunialensis* group extinction due to the absence of this group at Site 756.

In the following, the calcareous nannofossil bioevents identified in this study are discussed and listed in stratigraphic order. We do not further explore planktonic foraminifera events, except with respect to the stable isotope records (below).

The Top of *Discoaster barbadiensis* and *Discoaster saipanensis*

The extinction of *D. saipanensis* marks the base of Zone NP21 (Martini 1971), whereas the extinction of both *D. saipanensis* and *D. barbadiensis* are proposed to be used to mark the base of Subzone CP16a (Okada and Bukry 1980). In Agnini et al. (2014) the Top of *D. saipanensis* defines the base of Zone CNE21.

The Top of *D. saipanensis* (Pl. 3, Figs. 3-5) and *D. barbadiensis* (Pl. 3, Fig. 2) are calibrated at 34.44 Ma and 34.77 Ma, respectively (Blaj et al. 2009). As expected, at Hole 756C, the Top of *D. barbadiensis* and *D. saipanensis* occurred before the Eocene-Oligocene boundary (EOB), which was reported at 124.365 ± 0.13 mbsf. The Top of *D. saipanensis* is observed at a depth of 127.18 mbsf, whereas the Top of *D. barbadiensis* falls at a depth of 131.40 mbsf. This datum indicates that their extinctions are closely spaced.

The disappearance of these taxa dramatically modifies the discoaster assemblage that in the early Oligocene is characterized by a lower diversity and the dominance of few species ascribable to the flower-shape discoasters (e.g., *D. deflandrei, D. tanii* and *D. tanii nodifer*). These taxa will remain the dominant species within this genus for all the Oligocene and part of the Miocene (Young 1998).

The acme of *Clausiccocus subdistichus* group

290 At Hole 756C, we have merged *C. subdistichus* and *C. fenestratus* into a single informal group, named as *C.*
291 *subdistichus* group (Fig. 3). The Bc of *C. subdistichus* (Pl. 1, Figs. 13, 14) is considered a potential reliable
292 bioevent that allows to approximate quite well the Eocene-Oligocene boundary (EOB), being consistently
293 found in the upper part of Chron C13r (e.g., Tethyan region, Coccioni et al. 1988; Southern Ocean, Marino
294 and Flores 2002; Hyland et al. 2009; Equatorial Pacific, Toffanin et al. 2013; NW Atlantic, Norris et al. 2014).
295 In Agnini et al. (2014), the Bc of *C. subdistichus* (33.88 Ma) marks the base of Zone CN01 which corresponds
296 to upper Zone NP21. At Hole 756C, *C. subdistichus* becomes common and continuous (Bc) at 125.06 mbsf
297 shortly below the EOB (124.37 mbsf). The estimated age for the Bc of *C. subdistichus* at Hole 756C is slightly
298 older (34.03 Ma). It should be noted that the gradual and scattered increase in abundance of *C. subdistichus*
299 makes it difficult to properly recognize and place this event, making any site-to-site correlation challenging.
300 The end of the acme interval (Tc) of *Clausicoccus subdistichus* defines the base of the Subzone CP16b in
301 Okada and Bukry (1980). At ODP Hole 756C, the Tc of *C. subdistichus* is a neat event, characterized by a
302 sharp decrease in abundance of the species (from 166 to 23 n/mm^2), occurring at 118.00 mbsf and shortly
303 afterward the extinction (T) of *Ericsonia formosa* (119.38 mbsf). Our datum perfectly agrees with the ranking
304 reported for the Top of *E. obruta* (= *C. subdistichus*) by Backman (1987) in the South Atlantic.
305 However, this result is in disagreement with previous data indicating that the Tc of *C. subdistichus* (33.43 Ma)
306 should precede the disappearance of *E. formosa* (Berggren et al. 1995). Comparing all the data available, this
307 event displays a certain degree of discrepancy and further high-resolution investigations in different
308 depositional settings are needed in order to evaluate the reliability of the event, especially considering that
309 some of previous results are qualitative and/or use old poor-quality age models (Perch-Nielsen 1986, Moran
310 and Watkins 1988, Nocchi et al. 1988, Catanzariti et al. 1997).
311
312 **The Top of *Ericsonia formosa***
313 The Top of *Ericsonia formosa* defines the base of Zone NP22 and Subzone CP16c (Martini 1971, Okada and
314 Bukry 1980). The extinction of *E. formosa* (Pl. 1, Fig. 12) marks the base of Zone CNO2 and has an estimated
315 age of 32.92 Ma (Agnini et al. 2014). This biohorizon is generally easily recognizable in terms of abundance
316 decline (Backman 1987) and represents a highly reliable event at low-middle latitudes where it occurs between
317 the uppermost C13n and lower C12r (Berggren et al. 1995, Marino and Flores 2002). *Ericsonia formosa*
318 disappeared very early from the southern high latitudes, in association with the polarity Chronozone C18, and

thus is considered strongly diachronous between low-middle and high latitudes (Berggren et al. 1995). At ODP Hole 756C, *E. formosa* has a continuous and abundant pattern and its final extinction occurs at 119.38 mbsf. The observed abundance pattern compares well with previous data available from equatorial Pacific Ocean (Blaj et al. 2009, Toffanin et al. 2013) and South Atlantic (Bordiga et al. 2015) confirming the high reliability of this event. At Hole 756C, the disappearance of *E. formosa* precedes the Top common of *C. subdistichus*.

The Top of *Reticulofenestra umbilicus*

The disappearance of *R. umbilicus* (Pl. 1, Figs. 1, 2) defines the base of Zone CP17 and Zone NP23 (Martini 1971, Okada and Bukry 1980). In Agnini et al. (2014), the Top of *R. umbilicus* is used to define the base of Zone CNO3 and has an estimated age of 32.02 Ma. Zone CNO3 corresponds to the lower part of Zone NP23 (Martini 1971) and to Zone CP17 (Okada and Bukry 1980). This event is diachronous between low-middle and southern high latitudes (Berggren et al. 1995, Marino and Flores 2002).

At ODP Hole 756C, the abundance pattern of *R. umbilicus* shows a high variability, and the final part of its range is characterized by a gradual decrease with the last occurrence of the species observed at 116.11 mbsf. The Top of *R. umbilicus* could have potential use as a distinct bioevent, though the low abundances observed toward the end of its range could make the precise positioning of this biohorizon difficult.

The Base of *Sphenolithus distentus*

In Okada and Bukry (1980) the appearance (B) of *Sphenolithus distentus* (Pl. 3, Figs. 15-16) defines the base of Zone CP18, which corresponds in Martini (1971) to the upper part of Zone NP23. In Agnini et al. (2014), the Base of *S. distentus* marks the base of Zone CNO4 with an estimated age of 30.0 Ma. At ODP Hole 756C, the Base of *S. distentus* is recognized at 114.16 mbsf. It is worth noting that the close spacing between the Top of *R. umbilicus* (115.81 mbsf) and the Base of *S. distentus* (114.16 mbsf) indicate a decrease in LSR and a condensed Zone CP17.

3.2 Geochemical data

Bulk stable isotopes ($\delta^{13}C$ and $\delta^{18}O$) and calcium carbonate (% $CaCO_3$) have been compared along with deep sea benthic foraminifera (i.e., *Cibicidoides havanensis* and *Cibicidoides mundulus*) isotope data, calcareous nannofossil genera and diversity index (Fig. 4). Both bulk carbonate and benthic foraminiferal stable isotopes display the two-stepped oxygen isotope pattern described for complete successions (e.g., Hutchinson et al. 2021), suggesting that the EOT is well recorded at Ninetyeast Ridge.

Benthic stable isotope record. Benthic $\delta^{18}O$ varies between a 0.23‰ and 1.47‰, with a mean value of 0.91‰ and a standard deviation (σ) of 0.31‰ (Fig. 9). Overall, the $\delta^{18}O$ trend shows a progressive increase from the base of the section upward, with a first positive step (Step 1) starting at 127.1 mbsf and lasting up to 125.92 mbsf (initial increase of ~0.6 ‰). A second positive shift (EOIS) is located at 123.70 mbsf and ends at 122.71 mbsf (increase of 0.97‰). Above, $\delta^{18}O$ values remain relatively high and constant (122.71 mbsf - 120.4 mbsf), forming a plateau that is consistent with the EOGM (Earliest Oligocene Glacial Maximum; Hutchinson et al., 2021). Benthic $\delta^{13}C$ values range between 0.72‰ and 1.93‰ with a mean value of 1.24‰ ± 0.27‰ (σ).
Key features of the curve are a minimum in $\delta^{13}C$ at 126.40 mbsf (0.72 ‰), corresponding with a minimum in $\delta^{18}O$ (0.55‰), with $\delta^{13}C$ increasing thereafter in parallel with the stepped $\delta^{18}O$ pattern, to produce a temporary maximum in $\delta^{13}C$, as is typical in deep marine EOT records. Unlike the $\delta^{18}O$, from 122.30 mbsf the benthic $\delta^{13}C$ gradually returns to a new baseline of ca. 1-1.2‰. Shorter term variability in $\delta^{18}O$ and $\delta^{13}C$ on the order of 0.1-0.2‰, hints at cyclicity, although the resolution of the record is at the limits of being able to resolve this.

Bulk stable isotope record and carbonate content. The Hole 756C bulk carbonate $\delta^{18}O$ and $\delta^{13}C$ records are very similar to the benthic records in structure, although the absolute values are a little offset (0.18 and 0.31, respectively). Bulk $\delta^{18}O$ varies between 0.10‰ and 1.19‰, with a mean value of 0.73‰ ± 0.28‰ (σ).
$\delta^{13}C$ values range between 1.13‰ and 1.95‰ with a mean value of 1.55‰ and a standard deviation of ± 0.22‰. The mean $\delta^{18}O$ value (0.37‰) on the lower part of the study section (127.25-132.70 mbsf), is lower if compared with the average values calculated for rest of the section (0.80‰). The EOIS bulk $\delta^{18}O$ increase is much more pronounced compared to Step 1. Moreover, while $\delta^{18}O$ 'Step 1' is not apparent where we might expect it to be, there is a clear bulk $\delta^{13}C$ increase at the 'Step-1' level, as predicted using the nannofossil

definition of the base of the EOT (127.18 mbsf). In fact, like the benthic $\delta^{18}O$ record, if there is a 'Step-1' $\delta^{18}O$ increase it seems to occur at the base of Zone E21. Bulk $\delta^{13}C$ in contrast shows the same positive excursion centered around the EOGM as the benthic record.

The succession is characterized by generally high $CaCO_3$ content, ranging between 59% and 100%, with an average value of 81%. The high values documented during the early Oligocene are in agreement with previous data from the Pacific Ocean that have been interpreted as the result of a dramatic deepening of CCD and the consequent increased availability of carbonate sea water ions $(CO_3)^{2-}$ (Coxall et al. 2005), although due to much shallower paleodepths (ca. 400 m) it is unclear whether this relative increase in $CaCO_3$ is the result of ocean carbonate chemistry changes or changes in the contribution of other sediment types.

3.3 Planktonic assemblages

Planktonic foraminifera. The Hole 756C samples contain relatively diverse (20-30 species) assemblages of planktonic foraminifera. The most common species belong to the genera *Dentoglobigerina* and *Subbotina,* with *D. galavisi* and *S. utilusindex* being most common throughout the section. *Catapsydrax unicavus* and *Globorotaloides suteri* are additional common components. *Globigerinahteka index* (Pl. 4, Fig. 6) is abundant between 137.8-130.21 mbsf, accompanied by lower numbers of *G. tropicalis* and *G. luterbacheri*. Hantkeninids, represented by the species *H. alabamensis* (Pl. 4., Figs. 1-3) and *H. primitiva* only, are scarce and the *Turborotalita cerroazulensis-cunialensis* group, common elsewhere in the tropics and sub-tropics (Nocchi et al. 1986, Katz et al. 2008, Pearson et al. 2008, Edgar et al. 2020, Coxall et al. 2021, Wade et al. 2021) is virtually absent. The less angular/more globular relatives *Turborotalita ampliapertura* and *T. increbescens* are, however, common (Pl. 4, Figs. 8 and 9). The fine sand fraction 63-150 µm contains abundant *Chiloguembelina ototara* and common *Tenuitella gemma* throughout (Pl. 4, Figs. 10-14). In these respects, the Hole 756C assemblages appear transitional between the late Eocene-Oligocene Southern Ocean assemblages found on the Kerguelen Plateau (Huber 1991) and the more diverse tropical Indian Ocean assemblages (e.g., Pearson et al. 2008).

Calcareous nannofossils. Calcareous nannofossils are common to abundant throughout the studied interval, showing a general decrease in diversity (H index) in the Oligocene samples (Fig. 4). The Shannon's index values calculated for the study succession are relatively low ($0.84 \leq H \leq 2.40$). This is partially the result of

406 the fact that not all the specimens have been determined at species level, but rather grouped into larger
407 taxonomic units (see Appendix for details). However, the H index shows a certain degree of variability during
408 the EOT and a remarkable decline after the EOGM. The lower heterogeneity and evenness of the assemblages
409 during the Oligocene reflect a community structure with a few dominant taxa (*Reticulofenestra, Coccolithus*
410 and *Clausicoccus*). The preservation varies from moderate to good and dissolution and/or overgrowth seems
411 to have minimally affected the assemblages, as these processes are not pervasive in the study material.
412 There is no obvious change in preservation state through the section.
413 At ODP Hole 756C, *Reticulofenestra* is the dominant genus throughout all the studied interval (33.2-78.2%),
414 with a relative abundance showing a gradual and relatively small increasing trend toward the top of the
415 succession (Fig. 5). Conversely, *Coccolithus* (8.3-40.4%) displays an opposite trend with highly variable
416 abundances recorded across the EOT. *Cyclicargolithus* (0-2.76%) shows a gradual increase in abundance
417 across the EOT which persists throughout the lower Oligocene. *Clausicoccus*, *Dictyococcites* and
418 *Zyghrablithus* display similar abundances varying from 0 to ca. 20%. Specifically, *Clausicoccus* (0-20.8%;
419 primarily represented by *C. subdistichus* and *C. fenestratus*) displays a sudden peak of abundance (acme)
420 above the EOB followed by remarkable high values persisting during the EOGM.
421 *Dictyococcites* (0.6-14.0%) (*D. bisectus, D.* aff. *D. bisectus, D. hesslandii, D. filewiczii*) shows an increase in
422 abundance in the first step while the pattern becomes highly variable during the second step (EOIS) but overall,
423 it does not display any dramatic change in the study interval. *Zyghrablithus* (0-13.9%) is continuously present
424 and well preserved, the abundance pattern shows a general decrease across the EOT.
425 The most common taxon among *Sphenolithus* (0.9-8.7%) is *S. moriformis* group but the sphenolith
426 assemblages display relatively high diversity including *S. akropodus*, *S. predistentus, S. predistentus-distentus*
427 transitional forms*, S. distentus* and very sporadic occurrences of *S. radians, S. tribulosus* and *S. intercalaris*.
428 Genus *Ericsonia* (0-8.3 %) shows a general decrease in abundance across the two steps that eventually led to
429 its extinction. A minor but interesting component of the assemblages is *Lanternithus* (0-5%), which is rare and
430 scattered during the late Eocene and becomes more common and abundant in the early Oligocene.
431 Other genera that occurred less frequently are *Chiasmolithus* (0-3.2%), *Discoaster* (0-2.8%, mainly
432 represented by *D. tani gr.*) and *Isthmolithus* (0-2.62%). Discoasters are usually affected by diagenetic
433 overgrowth, and, thus, several specimens could not be confidently identified at species level.

Genera with sporadic occurrences have been reported as 'others' (0-5.8%) and include: *Coronocyclus, Helicosphaera, Pontosphaera, Thoracosphaera, Umbilicosphaera*, reworked and undetermined nannofossils.

3.4 Age-depth model

The age-depth model (Fig. 6) for the Eocene-Oligocene section of Hole 756C was developed using the position of calcareous nannofossil events with additional control provided by the top of the planktonic foraminifera *Hantkenina* and the Top of EOIS. Tie-points were placed at midpoints (mbsf) between bounding samples and their ages were assigned using the Geological Time Scale 2012 calibration ages (GTS12; Gradstein et al. 2012) (Table 1). The maximum LSR of 1.3 cm kyr^{-1} was recorded in the late Eocene (132.7-127.18 mbsf).

During the EOT and EOGM, we have recorded an average LSR of 0.6 cm kyr^{-1} (127.18-119.38 mbsf). Our data indicate a gradual decrease of LSRs during the Oligocene with LSR of 0.4 cm/kyr from 119.39 to 116.11 mbsf and a very low LSR of 0.1 cm kyr^{-1} in the upper interval (from 116.11 to 113.4 mbsf). If we assume that linear sedimentation rate has remained constant during this latter interval, this extremely low value of LSR (0.1 cm kyr^{-1}) denotes an extremely condensed Oligocene sequence. Otherwise, LSR might have been higher than the estimated value (>0.1 cm kyr^{-1}) during part of the range and zero for the remaining interval, inferring the presence of a hiatus. This second hypothesis is more feasible from a stratigraphic point of view since it could also account for the anomalous distribution of *Chiasmolithus altus* detected in the upper part of the section at this site. Based on the identified bioevents described above, the sedimentary section corresponds to the time interval from 34.86 to 29.27 Ma (5.6 Myr).

3.5 Principal component analysis

Our multivariate dataset consists of points (= samples) in a high multidimensional space projected down to a two-dimensional plot. The PCA analysis allows us to identify and interpret the axes of maximal variance (principal components) of our dataset, which are linear combinations of the original variables.

Results from PCA at ODP Hole 756C provide two significant principal component which explain 49.8% (PC1 27.88%; PC2 21.96%) of the total variance in our dataset. The screen plot reported in Fig. 7 shows where the variance explained (%) by each component starts to flatten out. Beyond that point, we have excluded the other components, that are possibly related to a "noise" component. The loadings of each component (PC1 and PC2 loadings) represent the contribution of each variable (% genus) to the component.

PC1 is positively loaded by *Ericsonia* (0.44), *Coccolithus* (0.38), *Discoaster* (0.34), *Zygrhablithus* (0.33), *Isthmolithus* (0.31) and negatively only by *Reticulofenestra* (-0.40) and *Cyclicargolithus* (-0.36).

The most meaningful genus loading on PC2 is *Lanternithus* (positively loading 0.51), but it is also loaded positively by *Clausicoccus* (0.47), *Chiasmolithus* (0.36) and *Sphenolithus* (0.35). PC2 is negatively loaded by *Coccolithus* (-0.24), *Reticulofenestra* (-0.24), *Ericsonia* (-0.19), *Discoaster* (-0.18). The loadings of the other genera are extremely low and are not further considered (Fig. 8).

A four-way separation of samples was used in order to recognize changes in the composition of the assemblage in the PCA biplot through time**:** late Eocene, EOT (defined by samples belonging to the E-O transition, Step 1 and EOIS), EOGM (samples characterized by maximum $\delta^{18}O$ values) and Oligocene (marked by samples above the EOGM) (Fig. 8).

4 Discussion

4.1 Site 756 stable isotope and biostratigraphy

In the few sites world-wide containing both the *Hantkenina* spp. extinction and having a reliable stable isotope record, the extinction of *Hantkenina* spp. has been found occurring between the two successive isotopic shifts (Coxall and Pearson 2007, Pearson et al. 2008, Hutchinson et al. 2021). The position of the Top of *Hantkenina* spp. at Hole 756C is generally in excellent agreement with previous data (Fig. 4), implying that while hantkeninids survived the ocean climate changes associated with the high-latitude cooling at Step 1 (Bohaty et al., 2012), they were unable to adapt to subsequent environmental disruptions. There is no temporary $\delta^{18}O$ increase in the late Eocene, suggesting that the 'late Eocene (glaciation) Event' found elsewhere (Hutchinson et al. 2021), is not recorded or falls in the interval of the coring/recovery gap at Site 756 (Fig. 4).

The benthic foraminifera $\delta^{18}O$ and $\delta^{13}C$ shows a rather clear signal of stepped isotopic change, with a magnitude comparable to other sites and consistent with the global ice volume increase (Hutchinson et al. 2021). Although bulk carbonate and benthic foraminifera $\delta^{18}O$ records show strong similarities (Fig. 4), minor offsets exist between these two signals. This is consistent with the idea that bulk carbonate stable isotopes primarily reflect mixed layer ocean conditions (Reghellin et al. 2015). In Hole 756C, the first bulk $\delta^{18}O$ increase (Step 1) is not as clear as that derived from benthic foraminiferal, suggesting limited sea-surface cooling at this step compared to the cooler deep waters bathing the seafloor. In contrast, the second positive

491 $\delta^{18}O$ shift (EOIS) is sharp and synchronous in both bulk and benthic foraminifera records, consistent with a
492 major ice expansion on Antarctica and significant glacial activity in the early Oligocene.
493
494 **4.2 Calcareous nannofossil biostratigraphy remarks**
495 The biozonations of Martini (1971) and Okada and Bukry (1980) are characterized by widely spaced
496 biohorizons. For this reason, quantitative distribution patterns of alternative taxa have been considered in this
497 work in order to provide supplementary bioevents across the EOT both for regional and worldwide
498 correlations. According to Fornaciari and Rio (1996), a biohorizon is reliable when it is easily reproducible
499 and identifiable by different workers and it can be systematically correlated over wide areas, maintaining the
500 same ranking and spacing. The taxa discussed in the following have been previously observed by different
501 authors but due to low abundances, poor preservation of the study material or lack of exhaustive studies, their
502 extrapolated ages are not confidently determined. These bioevents are reported in Table 1.
503 In some cases, distinct biohorizons are found to lie at the same stratigraphic position, as for example the Tc of
504 *C. subdistichus* and Tc of *L. minutus*. A reasonable explanation for this coincidence is possibly related to the
505 relatively low sedimentation rates at this specific interval of the study site.
506 The reliability and reproducibility of the examined bioevents are discussed below:
507
508 **The range of *Sphenolithus akropodus***
509 *Sphenolithus akropodus* was first described in north-eastern Atlantic Ocean sediments (Iberia Abyssal Plain)
510 as a relatively large species (7-9 μm) with a long elongated apical spine, sometimes bifurcated, and with short
511 proximal elements extending laterally to form a small base. At 0° to the crossed nicols, the apical spine is
512 weakly birefringent. In cross-polarized light at 45°, the apical spine is completely bright (de Kaenel and Villa
513 1996). In this work, we have observed two different morphotypes: *S. akropodus* morphotype A and *S.*
514 *akropodus* morphotype B that can be differentiated if observed at XPL at 0°. *S. akropodus* morphotype A (Pl.
515 3, figs. 7-8) is characterized by a single apical spine (not divided by a central extinction line), while *S.*
516 *akropodus* morphotype B (Pl. 3, figs. 9-10) shows an apical spine subdivided in two elements by a central
517 extinction line. Our data indicate overlapping abundance patterns for these morphotypes (Fig. 3), suggesting a
518 morphological variability within the same species, rather than intergradational forms.

519 At Hole 756C, the first appearance of this taxon is difficult to define due to its sporadic occurrence, but we
520 tentatively placed its base at 121.05 mbsf (33.29 Ma), within Zone NP21, equivalent to Zone CNO1 (Fig. 3).
521 Our datum is consistent with those provided by de Kaenel and Villa (1996), Bordiga et al. (2015) and more
522 recently by Villa et al. (2021), which indicate that this event occurs in the early Oligocene.
523 The base of *S. akropodus* could be used for a good approximation of this time interval, but further data are
524 required to confirm its reliability. The top of *S. akropodus* is found at 114.265 mbsf within Zone CNO3 (Agnini
525 et al. 2014), corresponding to the lower part of Zone NP23 of Martini (1971) and has an extrapolated age of
526 30.11 Ma.
527
528 **The Base common of *Sphenolithus predistentus***
529 At ODP Hole 756C, the species becomes common and continuous (Bc) up to 121.85 mbsf (estimated age of
530 33.46 Ma, early Oligocene), while data from the equatorial Indian Ocean (Fioroni et al. 2015) indicates that *S.*
531 *predistentus* is very abundant and commonly present already within Chron C13r (late Eocene).
532 The diachrony observed for this event suggests a low potential as possible additional bioevent. Specimens of
533 *S. predistentus* (Pl. 3, figs. 11-14) at ODP Hole 756C are relatively rare (0-31 n/mm^2, Fig. 3) and, in some
534 cases, this species is not easy to recognize essentially because of either (1) the absence of the two low quadrants
535 or 'feet' due to preservation issues, 2) taxonomic ambiguities between *S. predistentus* and *S. akropodus* (Bown
536 and Dunkley Jones 2012) or the presence of transitional forms (Blaj et al. 2010). For these reasons, and with
537 the available data, we do not recommend the use of the Bc of *S. predistentus.*
538
539 **The range of *Chiasmolithus altus***
540 At high latitudes, the biohorizons (Base and Top) related to *Chiasmolithus altus* are considered highly reliable
541 (Persico et al. 2008, Fioroni et al. 2012). At Hole 756C, the Base of *C. altus* (Pl. 1, figs 15, 16) was found at
542 123.21 mbsf (33.72 Ma) within Zone CNO1 (Fig. 3), in the lower Oligocene. This datum is consistent with
543 data reported from the Southern Ocean (Fioroni et al. 2012).
544 At 115.91 mbsf (31.81 Ma), *C. altus* becomes discontinuous and rare (Tc) shortly above the top of *R. umbilicus*
545 (within Zone CNO3). This datum differs from the known distribution of this species in the Oligocene (e.g.,
546 Villa et al. 2008, Fioroni et al. 2012) and could be most likely related to the presence of a hiatus, as mentioned
547 in paragraph 3.4. Data from the Southern Ocean document that *C. altus* first appears (Base) in the lower

548 Oligocene after an interval following the Top of *C. eoaltus* (or *C. altus-like*), a species restricted to the middle-
549 late Eocene (Persico and Villa 2008). *Chiasmolithus eoaltus* slightly morphologically differs from *C. altus*
550 Persico and Villa (2008) by having a larger central opening, a thinner rim, and one cross-bar not perfectly
551 aligned (i.e. slightly sigmoidal). Despite the overall moderate to good preservation of calcareous nannofossil
552 assemblages at Hole 756C, late Eocene specimens of *Chiasmolithus* are commonly affected by the absence or
553 heavy overgrowth of the cross-bar structure present in the central area, precluding, in some cases, the
554 unambiguous identification at a species level. The rarity of the taxon and the lack of the cross-bar structure
555 suggests caution in ascribing the forms observed in the middle-late Eocene to *C. eoaltus* and, consequently,
556 we referred to these specimens as *C. cf. eoaltus* (Fig. 3). Ultimately, the discrepancy observed between the
557 range of *C. altus* at Hole 756C with data from the Southern Ocean (Persico et al. 2008, Fioroni et al. 2012)
558 could be easily explained considering the subtropical location of the studied section.
559 The reliability of the Top common (Tc) and Base (B) of *Chiasmolithus altus* here presented requires further
560 investigations, especially in the low-middle latitudes, where these biohorizons have been poorly tested.
561
562 **'Top common of *Isthmolithus recurvus'* bioevent**
563 At ODP Hole 756C*, I. recurvus* (Pl. 2, figs. 6-7) displays a high variance in abundance (0-46 n/mm^2, Fig. 3),
564 but toward the end of its range it showed a neat decrease followed by a final discontinuous occurrence.
565 In our samples, *I. recurvus* is often overgrown, but thanks to its distinct shape it is still easily recognizable.
566 The final occurrence of this species at ODP Hole 756C is positioned at 116.51 mbsf (32.13 Ma) just below the
567 Top of *R. umbilicus* (116.11 mbsf). This finding is in agreement with previous estimations from mid latitudes
568 (Premoli Silva et al. 1988), as well as from the central equatorial Pacific (Lyle et al. 2002).
569 At low-middle latitudes (South Atlantic), Backman (1987) reported the extinction of this taxon below the Top
570 of *E. formosa*. In the Equatorial Indian Ocean (ODP 711), Fioroni et al. (2015) did not use this event, since *I.*
571 *recurvus* is extremely rare and poorly preserved in the studied material. The supposed diachroneity between
572 low and middle latitudes has been interpreted by Wei and Wise (1990) as related to a paleoecological
573 preference of this species for cool waters. In the studied section, *I. recurvus* shows a sharp drop at 122.25 mbsf
574 (33.55 Ma), which is used to define the 'Top' common occurrence of this species. The reliability of the 'Top
575 common of *I. recurvus'* remains debatable but future data will confirm or not the real potential of this
576 biohorizon.

577 **The acme of *Lanternithus minutus***

578 The abundance pattern of *Lanternithus minutus* (Pl. 2, Figs. 8-9) at Hole 756C (Fig. 5) is noteworthy for at
579 least three reasons: (1) there are only two high resolution datasets reporting the relative abundance pattern of
580 this taxon across the EOT (Dunkley Jones et al. 2008, Bordiga et al. 2015); (2) at ODP Hole 756C, the
581 abundance pattern of *L. minutus* is very similar to that of *C. subdistichus*; (3) in the study section, *L. minutus*
582 is well preserved although holococcoliths are generally considered to be particularly fragile and not easily
583 preserved in carbonate-rich pelagic sediments (Young et al. 2005, Bown et al. 2008, Dunkley Jones et al.
584 2008). At Hole 756C, *L. minutus* suddenly increases in abundance (acme) at 123.21 mbsf (33.72 Ma). This
585 change is used to mark the Bc of this taxon. The Top common of *L. minutus* is located at 118 mbsf (32.54 Ma)
586 and coincides with the Top common of *C. subdistichus*. Unluckily, the acme interval of *L. minutus* seems not
587 be a global feature, showing different patterns at different sites. In SE Atlantic Ocean (Bordiga et al. 2015),
588 this taxon shows an increase in abundance above EOIS (0-12% in abundance; dataset A), while data from
589 Tanzania (Dunkley Jones et al. 2008) reports an unrecoverable decline through the EOT.
590 *L. minutus* is not considered as a valuable biohorizon because of its high susceptibility to dissolution (especially
591 in deep waters) and the high vulnerability during diagenetic processes (Moran and Watkins 1988). Despite
592 these conflicting views, the species could be used as a paleoenvironmental indicator in regional contexts.
593

594 **4.3 Paleoenvironmental changes during the late Eocene – early Oligocene**

595 Calcareous nannofossils are excellent proxies for inferring paleoenvironmental reconstructions because of
596 their sensitivity to environmental conditions. Variations in calcareous nannofossil assemblages can be related
597 to changes in sea surface water temperature (SST), nutrient availability, intensity of solar radiance, salinity
598 and many other factors (e.g., Aubry 1992, Winter et al. 1994, Flores and Sierro 2013). However, the
599 complicated interaction between these abiotic parameters with the physical properties of the water masses (i.e.
600 upwelling, turbulence, stratification, and turbidity), atmospheric processes and biotic components (i.e.
601 competition, predation, disease, etc.) makes the disentangling of each contribution difficult.
602 In modern coccolithophore communities, sea water temperature is considered one of the most significant
603 parameters, playing a key role in defining the latitudinal distribution of species (Baumann et al. 2005).
604 Nevertheless, on more local scales, in modern tropical and subtropical regions, temperature variations seem to
605 be less informative and important (Andruleit et al. 2003). In these cases, what comes into play is another

606 fundamental parameter for coccolithophore growth and diversification: the availability of bio-limiting
607 nutrients. Despite the overall eurytopic nature of coccolithophores, taxa are subdivided in two different
608 ecological groups: k-specialist (oligotrophs, efficiency maximized, high H index) and r-opportunist (eutrophs,
609 grow rate maximized, low H index), although many species are considered to be mesotrophs (Bralower 2002).
610 Temperature and trophic conditions are often intimately correlated since eutrophic taxa are generally more
611 common in cold waters (high nutrients availability) and oligotrophic taxa are more abundant in warm waters
612 (low nutrients availability). To date, the ecological preferences of many species have received a wide
613 consensus among the scientific community, but others appear to have more complex and controversial
614 ecologies (Villa et al. 2008, Newsam et al. 2017).
615 At ODP Hole 756C, the PCA analysis was used to group coccolith taxa and to relate their temporal distribution
616 to the paleoecological structure of the upper photic zone (UPZ) during the E-O interval. From the analysis of
617 the major loading taxa, we tentatively correlate the changes observed in the assemblages with the main
618 paleoenvironmental parameters (principal components: PC1 and PC2). Major and minor loading taxa were
619 interpreted and compared in terms of temperature and trophic preferences with previously published
620 paleoecological assignments (Table 2). However, many taxa display broad ecological affinities and require
621 further study, as in the case of *Isthmolithus, Zygrhablithus, Sphenolithus* and *Dictyoccocites.* Their abundance
622 is likely the result of the complex interaction of abiotic and/or biotic parameters. For instance, the debate over
623 the apparently inconsistent ecological behavior of *Sphenolithus* and *Dictyoccocites* is probably related to the
624 fact that species belonging to these genera show species-specific responses, hampering any ecological
625 categorization at genus level (Langer et al. 2006, Toffanin et al. 2011, Cappelli et al. 2021).
626 According to our PCA results (Fig. 8), PC1 is positively loaded by *Coccolithus, Ericsonia, Discoaster,*
627 *Zygrablithus* and *Isthmolithus. Coccolithus* is thought to have changed its temperature preferences through
628 time, from warmer waters in the Paleogene to colder waters in the Neogene (Agnini et al. 2007). Pleistocene
629 and modern *C. pelagicus* prefer cold and/or eutrophic waters (Cachão and Moita 2000). At high latitudes, the
630 most abundant species of this genus, *C. pelagicus*, is considered to be indicative of temperate water conditions
631 during the Eocene-Oligocene transition (Wei and Wise 1990, Persico and Villa 2004, Villa et al. 2008).
632 *Ericsonia* is thought to have thrived in warm-waters in the Paleogene (Haq and Lohmann 1976, Wei and Wise
633 1990, Aubry 1992, Kelly et al. 1996, Bralower 2002) and is considered a warm water indicator (Villa et al.

2008, 2014, 2021). *Discoaster* has been consistently considered as a warm-water taxon, common in oligotrophic environments (Aubry 1998, Bralower 2002).

Finally, several studies have suggested that *Zygrablithus* is a near shore indicator (e.g., Heirtzler et al. 1977, Coccioni et al. 1988, Nocchi et al. 1988, Wei and Wise 1990, Monechi et al. 2000). However, the paleoecology of this taxon remains elusive based on the review reported in Villa et al. (2008), who highlighted highly inconsistent paleoecological affinities for *Z. bijugatus* among different authors. Our result possibly indicates a preference for warm and mesotrophic waters, but we are skeptical that the record of this taxon is only related to environmental conditions and rather support the hypothesis that diagenetic processes could have played an important role in favoring or disfavoring the preservation of this fragile taxon (Agnini et al. 2016). *Isthmolithus* has been interpreted as temperature-dependent taxon, with preferences for cool (Wei and Wise 1990, Wei et al. 1992, Monechi et al. 2000) or temperate waters (Persico and Villa 2004). In our opinion *Isthmolithus* ecological interpretation remains enigmatic. In the PCA biplot, *Isthmolithus recurvus* lies in the warm-oligotrophic field (Fig. 8) but this datum is essentially the result of the stratigraphic occurrence of this taxon that is not present in the early Oligocene, except in the lower part. The negative loadings on PC1 are *Reticulofenestra* and *Cyclicargolithus*. *Reticulofenestra* is an eurytopic cosmopolitan taxon, thriving in a wide range of environmental conditions with a preference for temperate waters (Wei and Wise 1990, Shcherbinina 2010, Cappelli et al. 2019), while *Cyclicargolithus floridanus* is considered a species with preferences for eutrophic-high productivity environments (Aubry 1992, Dunkley Jones et al. 2008, Villa et al. 2021).

PC2 is positively loaded by *Lanternithus, Clausicoccus, Chiasmolithus*, *Sphenolithus* and *Dictyococcites.*

The paleoecological preferences of *Lanternithus* (represented by *L. minutus*) are poorly known, nevertheless a number of studies have suggested that holococcoliths usually prefer more oligotrophic waters (Kleijne 1991, Winter et al. 1994, Cros et al. 2000, Baumann et al. 2005, Gibbs et al. 2006, Dunkley Jones et al. 2008, Bordiga et al. 2015). Nocchi et al. (1988) observed high abundances of *Lanternithus* and *Zygrablithus* in near shore settings and used these taxa as shallow-water indicators and cold-water tolerant species.

Our results seem to indicate eutrophic affinities for *Lanternithus* that is supported by the general increase in abundance observed starting with the middle Eocene, and the correlative eutrophication of the oceans (Agnini et al. 2006, Schneider et al. 2011, Cappelli et al. 2019). In general, the carbonate ocean chemistry together with local environmental conditions can possibly affect the preservation potential of holococcoliths and, in turn, their abundances (Young et al. 2005). However, the relatively shallow paleowater depth (~400 m) makes

663 Site 756 less prone to dissolution and thus the abundance pattern of *Lanternithus* potentially reflects a true
664 signal, not compromised by poor preservation. As regard to the paleoecology of *Clausicoccus*, Wei and Wise
665 (1990) reported a common presence of this taxon in the middle latitudes, though the distribution of this genus
666 may be controlled also by factors (e.g., nutrients, insolation, salinity) other than temperature. Our data suggest
667 a temperate-water affinity for this taxon, but also point out a strong control exerted by the high nutrient
668 availability in favoring the distribution of this species.
669 *Chiasmolithus* is thought to be indicative of cool-cold water conditions (Wei and Wise 1990, Wei et al. 1992
670 Bralower 2002, Persico and Villa 2004, Tremolada and Bralower 2004, Villa and Persico 2006, Villa et al.
671 2008), an ecological affinity that is confirmed in our study. Genus *Sphenolithus* is known to be considered a
672 warm water taxon (Villa et al. 2021) adapted to oligotrophic environments (Aubry 1998, Bralower 2002, Gibbs
673 et al. 2004, Kalb and Bralower 2012), even so the study carried out by Wade and Bown (2006) shows a strong
674 increase of sphenoliths during eutrophic conditions. It is becoming increasingly evident that species belonging
675 to the same genus can in fact better thrive in a wide trophic continuum (Dunkley Jones et al. 2008, Toffanin et
676 al. 2011, Cappelli et al 2021) showing species-specific responses to climate/environmental changes. In this
677 view the constant abundance displayed at genus level (Fig. 5) blurs the more nuanced ecological preferences
678 at species level, where *S. akropodus* and *S. predistentus* partially substitute the warm-oligotrophic *S.*
679 *moriformis* during the EOT, suggesting a more eutrophic/temperate affinity for the former taxa. The
680 paleoecological affinities of *Dictyococcites* are still under debate and this is essentially due to the controversial
681 taxonomy of this group and insufficient data available. For instance, different preferences have been proposed
682 for *D. bisectus* which is designated as a temperate-water (Persico and Villa 2004), warm to temperate (Wei
683 and Wise 1990) or warm taxon (Monechi et al. 2000). The PCA results suggest a temperate/mesotrophic
684 affinities with different species possibly lying in a different position of the trophic resource continuum (TRC;
685 Hallock 1987). Based on these considerations, PC1 (27.88% of the total variance) and PC2 (21.96% of the
686 total variance) were distinguished as representative, respectively, of paleotemperature and trophic conditions.
687 According to our paleoecological interpretation, calcareous nannofossil taxa are, when possible and supported
688 by straightforward data, subdivided in three eco-groups:
689 1) **Warm-oligotrophic group**, that includes *Coccolithus, Ericsonia, Discoaster,* characterized by warm
690 temperatures (high PC1 scores) and low nutrients affinity (low PC2 scores).
691 2) **Temperate-eutrophic group**, to which belong *Clausicoccus, Lanternithus* and *Chiasmolithus*.

692 This eco-group is characterized by high trophic (high PC2 scores) and intermediate temperatures
693 preferences. Within these groups, *Clausicoccus* and *Lanternithus* seems to be highly sensitive to
694 trophic conditions and their peaks in abundance across the EOGM were probably induced by a high
695 availability of nutrients.
696 3) **Cold-mesotrophic group** that comprises *Reticulofenestra* and *Cyclicargolithus* genera characterized
697 by low temperature and a return to slightly oligotrophic paleoenvironmental conditions.
698 The following taxa have been excluded from the three main eco-groups because of more difficult interpretation
699 and include: *Zygrhablithus* (warm-mesotrophic), *Dictyococcites* (temperate-mesotrophic; species-specific
700 affinities), *Sphenolithus* (species-specific affinities) and *Isthmolithus,* for which we require further
701 investigations.
702
703 **4.4 Comparison with other nannofossil studies**
704 At Hole 756C, the loss of the warm-oligotrophic community is one the main changes observed in the
705 nannoplankton assemblage, together with the massive increase of the temperate-eutrophic taxa (*Clausicoccus*,
706 *Chiasmolithus* and *Lanternithus*) closely coupled to the EOIS and the EOGM (Fig. 8A). No specific
707 assemblage response was observed at Step 1. Instead, the only significant change that occurred close to the
708 EOB, is a remarkable increase of abundance (acme) of *Clausicoccus*.
709 Our data suggest that the causes of calcareous nannofossil changes at ODP Hole 756C are related to both
710 temperature and trophic conditions, in agreement with previous studies from low-middle latitudes (Dunkley
711 Jones et al. 2008, Jones et al. 2019, Villa et al. 2021). Specifically, if compared with the record available from
712 Tanzania (Dunkley Jones et al. 2008) our data similarly record an increase in the relative abundance of *C.*
713 *floridanus* and *S. predistentus,* but important differences have been observed with regard to holococcolith
714 abundances. While our dataset displays an unusual increase in abundance of *L. minutus,* the record from
715 Tanzania indicates a marked reduction of holococcoliths (i.e. *Varolia macleodi, Lanternithus minutus* and
716 *Zygrhablithus bijugatus*) during the E-O transition. The overall comparison with other low-middle latitude
717 datasets (Tanzania; Dunkley Jones et al. 2008; Equatorial Indian Ocean; Fioroni et al. 2015; Villa et al. 2021
718 and Indo-Pacific; Jones et al. 2019; Equatorial Pacific; Blaj et al. 2009) highlights important similarities and a
719 substantial synchronicity in the changes documented in the calcareous nannofossil record.

720 Noteworthy, the abundance pattern of *I. recurvus* recorded in the Southern Kerguelen Plateau (Site 748; Wei
721 et al. 1992, Villa et al. 2008) is similar to our record (0-3%) and differs from that recorded in the Equatorial
722 Indian Ocean (Sites 711, 709; Fioroni et al. 2015, Villa et al. 2021), where this species is strongly reduced or
723 virtually absent. Similarly, limited *Chiasmolithus* and *Reticulofenestra daviesii* were recorded, in contrast to
724 much higher abundances documented in the Kerguelen Plateau (Wei et al. 1992, Villa et al. 2008) and to the
725 rarity or absence of these taxa in the Equatorial Indian Ocean (Wei et al. 1992, Fioroni et al. 2015, Villa et al.
726 2021). Thus, as observed for the planktonic foraminifera assemblages, at Hole 756C, the E-O calcareous
727 nannofossil assemblages appear transitional between the assemblages found on the Kerguelen Plateau (Wei et
728 al. 1992) and from the Equatorial Indian Ocean (Fioroni et al. 2015, Villa et al. 2021).
729 The water masses formed in the Southern Ocean and flowing northward were characterized by low temperature
730 and high nutrients levels (Sarmiento et al. 2004). The deep circulation of these water masses was likely
731 invigorated close to the EOT providing an enhanced nutrient supply at low-middle latitudes which eventually
732 leads to more eutrophic conditions in the Indian Ocean (Villa et al. 2021). As a result, the transition from the
733 Eocene to the Oligocene was marked by a progressive increase in abundance of opportunistic taxa better
734 adapted to thrive in cooler and more eutrophic environments (Dunkley Jones et al. 2008, Fioroni et al. 2015,
735 Jones et al. 2019, Villa et al. 2021). Other than changes in ocean circulation, an alternative possible explanation
736 for the eutrophic conditions recorded at ODP Hole 756C likely involved the weathering of shelf sediments in
737 response to sea level fall (e.g., Merico et al. 2008), but the paleoceanographic changes that occurred in the
738 Antarctic area remain the most plausible mechanisms to explain all the modification observed in calcareous
739 nannofossils. Moreover, our paleoproductivity proxy (PC2 scores; Fig. 8B) also highlights the presence of a
740 transient and large increase in nutrients coeval with the global maximum $\delta^{18}O$ values (EOGM) and major ice
741 build-up on Antarctica. Our interpretation is that this temporary nutrient overshoot, might have been caused
742 by an additional short-term event, such as a sudden and massive input of micro-nutrients to the ocean due to
743 maximum glacial expansion in the earliest Oligocene (Diester-Haass and Zahn 1996).
744
745 **4.5 The paleoecological significance of *Reticulofenestra***
746 *Reticulofenestra* is thought to be a cosmopolitan taxon, but different species or informal groups ascribed to
747 this genus can lie in different positions of TRC. For this reason and, in order to better constrain their
748 paleoecological significance, we decide to consider them separately. Our results indicate a long-term decrease

749 in relative abundance (%) of medium to large reticulofenestrids (*Reticulofenestra* spp. 10-14 μm and
750 *Reticulofenestra umbilicus* >14 μm) starting in the late Eocene and culminating after the EOT. This group was
751 replaced by small-sized reticulofenestrids (*Reticulofenestra* spp. 4-10 μm), which show a remarkable increase
752 after the EOGM (Fig. 9). The decrease in size of *Reticulofenestra* perfectly matches with the SST
753 paleoenvironmental proxy (derived from PC1), confirming a temperature-dependence of this group. A possible
754 explanation is that larger reticulofenestrids were probably better adapted to warmer Eocene sea-surface
755 temperatures, while smaller forms were more competitive in Oligocene cold waters. Moreover, this
756 macroevolutionary size-decrease reflects the long-term decline of pCO_2: the bio-limiting levels of $[CO_2]_{aq}$
757 characterizing the surface waters during the Oligocene have likely reduced the diffusive CO_2 uptake of larger
758 reticulofenestrids (low SA:V ratio) with a competitive advantage for smaller forms (high SA:V ratio)
759 (Henderiks and Pagani 2008).
760 Finally, among reticulofenestrids, *Rerticulofenestra daviesii* displays a complex behavior. The abundance
761 pattern of this species suggests a wide temperature tolerance as proposed by Bordiga et al. (2017).
762 Nevertheless, the high abundance observed across the EOT is possibly a response to the eutrophic conditions
763 inferred for this interval and is consistent with the eutrophic ecological affinity recently proposed for this taxon
764 (Villa et al. 2014, 2021). In addition, we should also consider the importance of the competitive dynamics
765 within a biological community in regulating the ecological success or failure of a group/taxon. In this regard,
766 at ODP Hole 756C, *R. daviesii* appears to be less competitive as small reticulofenestrids, especially after the
767 EOGM and could have been ecologically marginalized by these forms, as well as the larger reticulofenestrids
768 in the late Eocene.
769
770
771
772
773
774
775
776
777

5 Conclusions

Our integrated benthic foraminifera and bulk stable isotope stratigraphies, and nannofossil and planktonic foraminifera biostratigraphies across the late Eocene and early Oligocene of Indian Ocean ODP Hole 756C, demonstrate well-defined and familiar geochemical structure within a consistent relative chronological framework. These constraints make Site 756 an excellent site for exploring pelagic changes in the subtropical Indian Ocean during the greenhouse to icehouse transition. An important aspect of Site 756 is that the shallow water depths facilitate good planktonic foraminifera as well as nannofossil preservation, and this includes preservation of the E/O boundary marker genus *Hantkenina*. The extinction of *Hantkenina* spp. in Hole 756C at 124.4 mbsf, occurs during an intermediate plateau between positive $\delta^{18}O$ and $\delta^{13}C$ isotopic shifts, as has been shown elsewhere. This is the first open-ocean Indian Ocean record to demonstrate this pattern, confirming the global synchroneity of this extinction event with respect to the familiar sequence of ocean-climate changes occurring during the EOT.

The new integrated isotopic and biostratigraphic framework allows a detailed examination of nannofossil assemblage variability at Hole 756C, leading to further refinements to local and potentially global EOT nannofossil biostratigraphy and nannofossil palaeoceanographic interpretations. The biostratigraphy of Indian Ocean ODP Hole 756C has been refined based on a semi-quantitative high-resolution calcareous nannofossil record across the E-O transition. This study confirms the reliability of classical or already known bioevents, but we also present new alternative biohorizons, which possibly implement the overall biostratigraphic framework of this interval: the acme of *Clausicoccus subdistichus* gr. and *Lanternithus minutus*, the total range of *Sphenolithus akropodus* and *Chiasmolithus altus* and the Tc of *Isthmolithus recurvus*, at least at regional scale. During the late Eocene/early Oligocene transition, calcareous nannofossil assemblages underwent an abrupt turnover with a permanent decline of warm-oligotrophic taxa, a decrease in species diversity and a remarkable increase in eutrophic taxa. We interpret this profound reorganization in nannoplankton assemblage as the result of two major paleoenvironmental changes: a decrease in SST coupled with an increase in nutrient availability. We hypothesize that the new paleoenvironmental conditions likely favored the expansion of temperate/cold water taxa better adapted to a nutrient-rich environment at the expense of warm-water oligotrophic taxa. Our multivariate analysis suggests a main disruption in the taxonomic composition of the assemblage between the EOT and EOGM triggered by enhanced nutrient levels.

This interpretation is further corroborated by strong evidence of invigorated ocean circulation that might be able to transport colder and nutrient-enriched waters at low-middle latitudes (Diester-Haass and Zachos 2003, Dunkley Jones et al. 2008, Coxall and Wilson 2011, Fioroni et al. 2015, Jones et al. 2019, Villa et al. 2021). Beyond the overall eutrophication recorded across the EOT, a transient and large nutrient overshoot was recorded at the EOGM, as supported by the high relative abundance of the temperate-eutrophic eco-group.

In a long-term perspective, smaller reticulofenestrids gradually increase across the E-O transition to the detriment of the larger forms, which display an opposite decreasing trend.

Acknowledgements

The authors are grateful to the Integrated Ocean Drilling Program (IODP) for providing samples and data used in this study. The IODP is sponsored by the U.S. National Science Foundation (NSF) and participating countries under the management of Joint Oceanographic Institutions, Inc. Thanks to Elias Chadli for planktonic foraminifera sample washing and benthic foraminifera stable isotope picking and to Heike Sigmund for stable isotope analysis at Stockholm University. We sincerely thank Paul Pearson for his insightful comments on the manuscript. Isabella Raffi and Davide Persico are deeply thanked for their constructive comments in the capacity of reviewers of A.V.' s PhD thesis during the evaluation process required by Italian law.

A. V. and C. A. were supported by University of Padova.

Supplementary data to this article will be stored in the PANGAEA database (Dataset S1 to S6).

Appendix. Taxonomic list

References

Abelson, M., Erez, J., 2017. The onset of modern-like Atlantic meridional overturning circulation at the Eocene-Oligocene transition: Evidence, causes, and possible implications for global cooling. Geochemistry, Geophysics, Geosystems 18, 2177–2199.

Agnini, C., Fornaciari, E., Raffi, I., Catanzariti, R., Pälike, H., Backman, J., Rio, D., 2014. Biozonation and biochronology of Paleogene calcareous nannofossils from low and middle latitudes. Newsletters on Stratigraphy 47, 131–181.

Agnini, C., Fornaciari, E., Rio, D., Tateo, F., Backman, J., Giusberti, L., 2007. Responses of calcareous nannofossil assemblages, mineralogy and geochemistry to the environmental perturbations across the Paleocene/Eocene boundary in the Venetian Pre-Alps. Marine Micropaleontology 63, 19–38.

Agnini, C., Muttoni, G., Kent, D. V., Rio, D., 2006. Eocene biostratigraphy and magnetic stratigraphy from Possagno, Italy: The calcareous nannofossil response to climate variability. Earth and Planetary Science Letters 241, 815–830.

Agnini, C., Spofforth, D.J.A., Dickens, G.R., Rio, D., Pälike, H., Backman, J., Muttoni, G., Dallanave, E., 2016. Stable isotope and calcareous nannofossil assemblage record of the late Paleocene and early Eocene (Cicogna section). Climate of the Past 12, 883–909.

Andruleit, H., Stäger, S., Rogalla, U., Čepek, P., 2003. Living coccolithophores in the northern Arabian Sea: ecological tolerances and environmental control. Marine Micropaleontology 49, 157–181.

Armstrong Mckay, D.I., Tyrrell, T., Wilson, P.A., 2016. Global carbon cycle perturbation across the Eocene-Oligocene climate transition. Paleoceanography 31, 311–329.

Aubry, M.-P., 1984. Handbook of Cenozoic calcareous nannoplankton, book 1, Ortholithae (Discoaster). American Museum of Natural History Micropaleontology Press, New York.

Aubry, M.-P., 1988. Handbook of Cenozoic calcareous nannoplankton, book 2, Ortholithae (Holococcoliths, Ceratoliths and others). American Museum of Natural History Micropaleontology Press, New York.

Aubry, M.-P., 1989. Handbook of Cenozoic Calcareous Nannoplankton, book 3, Ortholithae (Pentaliths, and Others) Heliolithae (Fasciculiths, Sphenoliths and Others). American Museum of Natural History Micropaleontology Press., New York.

Aubry, M.-P., 1992. Late Paleogene Calcareous Nannoplankton Evolution: A Tale of Climatic Deterioration. In: Eocene-Oligocene Climatic and Biotic Evolution, p. 272–279.

865 Aubry, M.-P., 1998. Early Paleogene Calcareous nannoplankton evolution: a tale of climatic amelioration. In:
866 Aubry, M.-P., et al. (Eds.), Late Paleocene–Early Eocene Biotic and Climatic Events in the Marine and
867 Terrestrial Records. Columbia University Press, New York, p. 158–201.
868 Backman, J., 1987. Quantitative Calcareous Nannofossil Biochronology of Middle Eocene through Early
869 Oligocene Sediment from DSDP Sites 522 and 523. Abhandlungen der Geologischen Bundesanstalt 39,
870 21–31.
871 Backman, J., Hermelin, J.O.R., 1986. Morphometry of the Eocene nannofossil Reticulofenestra umbilicus
872 lineage and its biochronological consequences. Palaeogeography, Palaeoclimatology, Palaeoecology 57,
873 103–116.
874 Backman, J., Raffi, I., Rio, D., Fornaciari, E., Pälike, H., 2012. Biozonation and biochronology of Miocene
875 through Pleistocene calcareous nannofossils from low and middle latitudes. Newsletters on Stratigraphy
876 45, 221–244.
877 Backman, J., Shackleton, N.J., 1983. Quantitative biochronology of Pliocene and early Pleistocene calcareous
878 nannofossils from the Atlantic, Indian and Pacific oceans. Marine Micropaleontology 8, 141–170.
879 Baldauf, J.G., 1992. Middle Eocene through early Miocene diatom floral turnover. In: Prothero, D.R.,
880 Berggren, W.A. (Eds.), Eocene–Oligocene Climatic and Biotic Evolution. Princeton University Press,
881 Princeton, NJ.
882 Baumann, K.-H., Andruleit, H., Bockel, B., Geisen, M., Kinkel, H., 2005. The significance of extant
883 coccolithophores as indicators of ocean water masses, surface water temperature, and paleoproductivity:
884 a review. Paläontologische Zeitschrift 79, 93–112.
885 Berggren, W.A., Kent, D. V., Swisher, C.C., Aubry, M.-P., 1995. A Revised Cenozoic geochronology and
886 chronostratigraphy. In: Berggren, W. A., Kent, D.V., Aubry, M.-P., Hardenbol, J. (Eds.), Geochronology,
887 Time Scales, and Global Stratigraphic Correlation: A Unified Temporal Framework for an Historical
888 Geology. Special publication - Society of Economic Paleontologists and Mineralogists, p. 129–212.
889 Blaj, T., Backman, J., Raffi, I., 2009. Late Eocene to Oligocene preservation history and biochronology of
890 calcareous nannofossils from paleo-equatorial Pacific Ocean sediments. Rivista Italiana di Paleontologia
891 e Stratigrafia 115, 67–85.
892 Blaj, T., Henderiks, J., Young, J.R., Rehnberg, E., 2010. The Oligocene nannolith Sphenolithus evolutionary
893 lineage: morphometrical insights from the palaeo-equatorial Pacific Ocean. Journal of

Micropalaeontology 29, 17–35.

Bohaty, S.M., Zachos, J.C., Delaney, M.L., 2012. Foraminiferal Mg/Ca evidence for Southern Ocean cooling across the Eocene-Oligocene transition. Earth and Planetary Science Letters 317-318, 251–261.

Bordiga, M., Henderiks, J., Tori, F., Monechi, S., Fenero, R., Legarda-Lisarri, A., Thomas, E., 2015. Microfossil evidence for trophic changes during the Eocene-Oligocene transition in the South Atlantic (ODP Site 1263, Walvis Ridge). Climate of the Past 11, 1249–1270.

Bordiga, M., Sulas, C., Henderiks, J., 2017. Reticulofenestra daviesii: biostratigraphy and paleogeographic distribution across the Eocene–Oligocene boundary. Geobios 50, 349–358.

Bown, P.R., 2005. Paleogene calcareous nannofossils from the Kilwa and Lindi areas of coastal Tanzania (Tanzania Drilling Project 2003-4). Journal of Nannoplankton Research 27, 21–95.

Bown, P.R., Dunkley Jones, T., 2012. Calcareous nannofossils from the Paleogene equatorial Pacific (IODP Expedition 320 Sites U1331-1334). Journal of Nannoplankton Research 32, 3–51.

Bown, P.R., Dunkley Jones, T., Lees, J.A., Randell, R.D., Mizzi, J.A., Pearson, P.N., Coxall, H.K., Young, J.R., Nicholas, C.J., Karega, A., Singano, J.M., Wade, B.S., 2008. A Paleogene calcareous microfossil Konservat-Lagerstätte from the Kilwa Group of coastal Tanzania. Geological Society of America Bulletin 120, 3–12.

Bown, P.R., Newsam, C., 2017. Calcareous nannofossils from the Eocene North Atlantic Ocean (IODP Expedition 342 Sites U1403–1411). Journal of Nannoplankton Research 37, 25–60.

Bown, P.R., Young, J.R., 1998. Techniques. In: Bown, P.R. (Ed.), Calcareous Nannofossil Biostratigraphy. Kluwer Academic Publishers, London, p. 16–28.

Bralower, T.J., 2002. Evidence of surface water oligotrophy during the Paleocene-Eocene Thermal Maximum: nannofossil assemblage data from Ocean Drilling Program Site 690, Maud Rise, Weddell Sea. Paleoceanography 17, 1023.

Cachão, M., Moita, M.T., 2000. Coccolithus pelagicus, a productivity proxy related to moderate fronts off Western Iberia. Marine Micropaleontology 39, 131–155.

Cappelli, C., Bown, P.R., de Riu, M., Agnini, C., 2021. The evolution of Eocene (Ypresian/Lutetian) sphenoliths: biostratigraphic implications and paleoceanographic significance from North Atlantic Site IODP U1410. Newsletters on Stratigraphy 54 (4), 405-431.

Cappelli, C., Bown, P.R., Westerhold, T., Bohaty, S.M., De Riu, M., Lobba, V., Yamamoto, Y., Agnini, C.,

2019. The early to middle Eocene transition: an integrated calcareous nannofossil and stable isotope record from the Northwest Atlantic Ocean (IODP Site U1410). Paleoceanography and Paleoclimatology 34, 1–18.

Catanzariti, R., Rio, D., Martelli, L., 1997. Late Eocene to Oligocene calcareous nannofossil Biostratigraphy in Northern Apennines: the Ranzano sandstone. Memorie di Scienze Geologiche 49, 207–253.

Coccioni, R., Monaco, P., Monechi, S., Nocchi, M., Parisi, G., 1988. Biostratigraphy of the Eocene-Oligocene bonudary at Massignano (Ancona, Italy). In: Premoli Silva, I., Coccioni, R., Montanari, A. (Eds.), The Eocene–Oligocene Boundary in the March-Umbria Basin (Italy). Fratelli Anniballi, Ancona, p. 81–96.

Coplen, T.B., Brand, W.A., Gehre, M., Gröning, M., Meijer, H.A.J., Toman, B., Verkouteren, R.M., 2006. New guidelines for $\delta^{13}C$ measurements. Analytical Chemistry 78, 2439–2441.

Cotton, L.J., Pearson, P.N., 2011. Extinction of larger benthic foraminifera at the Eocene/Oligocene boundary. Palaeogeography, Palaeoclimatology, Palaeoecology 311, 281–296.

Coxall, H.K., Huck, C.E., Huber, M., Lear, C.H., Legarda-lisarri, A., Regan, M.O., Sliwinska, K.K., Flierdt, T. Van De, Boer, A.M. De, Zachos, J.C., O'Regan, M., Sliwinska, K.K., Van De Flierdt, T., De Boer, A.M., Zachos, J.C., Backman, J., 2018. Export of nutrient rich Northern Component Water preceded early Oligocene Antarctic glaciation. Nature Geoscience 11, 190–196.

Coxall, H.K., Dunkley Jones, T., Jones, A.P., Lunt, P., MacMillan, I., Marliyani, G.I., Nicholas, C.J., O'Halloran, A., Piga, E., Sanyoto, P., Rahardjo, W., Pearson, P.N., 2021. The Eocene−Oligocene transition in Nanggulan, Java: lithostratigraphy, biostratigraphy and foraminiferal stable isotopes. Journal of the Geological Society, 178 (6).

Coxall, H.K., Pearson, P.N., 2007. The Eocene-Oligocene Transition. In: Williams, M., Haywood, A.M., Gregory, J., Schmidt, D.N. (Eds.), Deep-Time Perspectives on Climate Change: Marrying the Signal from Computer Models and Biological Proxies, Micropaleontology Society Special Publication. Geological Society, London, p. 351–387.

Coxall, H.K., Wilson, P.A., 2011. Early Oligocene glaciation and productivity in the eastern equatorial Pacific: Insights into global carbon cycling. Paleoceanography 26, 1–18.

Coxall, H.K., Wilson, P.A., Pälike, H., Lear, C.H., Backman, J., 2005. Rapid stepwise onset of Antarctic glaciation and deeper calcite compensation in the Pacific Ocean. Nature 433, 53–7.

Cros, L., Kleijne, A., Zeltner, A., Billard, C., Young, J.R., 2000. New examples of holococcolith-

heterococcolith combination coccospheres and their implications for coccolithophorid biology. Marine Micropaleontology 39, 1–34.

Davies, R., Cartwright, J., Pike, J., Line, C., 2001. Early Oligocene initiation of North Atlantic Deep Water formation. Nature 410, 917–920.

de Kaenel, E., Villa, G., 1996. Oligocene Miocene calcareous nannofossil biostratigraphy and paleoecology from the Iberia Abyssal plain. Proceedings of the Ocean Drilling Program, Scientific results 149, 79–145.

DeConto, R.M., Pollard, D., 2003. Rapid Cenozoic glaciation of Antarctica induced by declining atmospheric CO_2. Nature 1317, 1313–1317.

Diester-Haass, L., Zachos, J.C., 2003. The Eocene-Oligocene transition in the Equatorial Atlantic (ODP Site 925); Paleoproductivity increase and positive $\delta^{13}C$ excursion. In: Prothero, D.R., Ivany, C.L., Nesbitt, E.A. (Eds.), From Greenhouse to Icehouse; The Marine Eocene-Oligocene Transition. Columbia Univ. Press, New York, NY, USA, p. 397–416.

Diester-Haass, L., Zahn, R., 2001. Paleoproductivity increase at the Eocene - Oligocene climatic transition: ODP/DSDP sites 763 and 592. Palaeogeography, Palaeoclimatology, Palaeoecology 172, 153–170.

Diester-Haass, L., Zahn, R., 1996. Eocene-Oligocene transition in the Southern Ocean: History of water mass circulation and biological productivity. Geology 24, 163–166.

Dunkley Jones, T., Bown, P.R., Pearson, P.N., Wade, B.S., Coxall, H.K., Lear, C.H., 2008. Major shifts in calcareous phytoplankton assemblages through the Eocene-Oligocene transition of Tanzania and their implications for low-latitude primary production. Paleoceanography 23, 1–14.

Edgar, K.M., Bohaty, S.M., Coxall, H.K., Bown, P.R., Batenburg, S.J., Lear, C.H., Pearson, P.N., 2020. New composite bio- And isotope stratigraphies spanning the Middle Eocene Climatic Optimum at tropical ODP Site 865 in the Pacific Ocean. Journal of Micropalaeontology 39, 117–138.

Egan, K.E., Rickaby, R.E.M., Hendry, K.R., Halliday, A.N., 2013. Opening the gateways for diatoms primes Earth for Antarctic glaciation. Earth and Planetary Science Letters 375, 34–43.

Fioroni, C., Villa, G., Persico, D., Jovane, L., 2015. Middle Eocene-Lower Oligocene calcareous nannofossil biostratigraphy and paleoceanographic implications from Site 711 (equatorial Indian Ocean). Marine Micropaleontology 118, 50–62.

Fioroni, C., Villa, G., Persico, D., Wise, S.W., Pea, L., 2012. Revised middle Eocene-upper Oligocene

calcareous nannofossil biozonation for the Southern Ocean. Revue de Micropaleontologie 55, 53-70.

Flores, J.A., Sierro, F.J., 2013. Coccolithophores. In: Encyclopedia of Quaternary Science. p. 783–794.

Fontorbe, G., Frings, P.J., De La Rocha, C.L., Hendry, K.R., Carstensen, J., Conley, D.J., 2017. Enrichment of dissolved silica in the deep equatorial Pacific during the Eocene-Oligocene. Paleoceanography 32, 848–863.

Fornaciari, E., Agnini, C., Catanzariti, R., Rio, D., Bolla, E.M.E.M., Valvasoni, E., 2010. Mid-latitude calcareous nannofossil biostratigraphy and biochronology across the middle to late eocene transition. Stratigraphy 7, 229–264.

Fornaciari, E., Rio, D., 1996. Latest Oligocene to Early Middle Miocene Quantitative Calcareous Nannofossil Biostratigraphy in the Mediterranean Region. Micropaleontology 42, 1–36.

Funakawa, S., Nishi, H., Moore, T.C., Nigrini, C.A., 2006. Radiolarian faunal turnover and paleoceanographic change around Eocene/Oligocene boundary in the central equatorial Pacific, ODP Leg 199, Holes 1218A, 1219A, and 1220A. Palaeogeography, Palaeoclimatology, Palaeoecology 230, 183–203.

Gibbs, S.J., Bralower, T.J., Bown, P.R., Zachos, J.C., Bybell, L.M., 2006. Shelf and open-ocean calcareous phytoplankton assemblages across the Paleocene-Eocene thermal maximum: Implications for global productivity gradients. Geology 34, 233–236.

Gibbs, S.J., Shackleton, N.J., Young, J.R., 2004. Orbitally forced climate signals in mid-Pliocene nannofossil assemblages. Marine Micropaleontology 51, 39–56.

Gradstein, F.M., Ogg, J.G., Schmitz, M.D., Ogg, G.M., 2012. The Geologic Time Scale 2012. Elsevier, Amsterdam, Netherlands.

Hallock, P., 1987. Fluctuations in the trophic resource continuum: A factor in global diversity cycles? Paleoceanography 2, 457–471.

Hammer, Ø., Harper, D.T., 2006. Paleontological data analysis. Blackwell publishing, Malden, USA.

Hammer, Ø., Harper, D.T., Ryan, D.D., 2001. Past: Paleontological Statistics Software Package for Education and Data Analysis. Palaeontologia Electronica 4, 5–7.

Haq, B.U., Lohmann, G.P., 1976. Early Cenozoic calcareous nannoplankton biogeography of the Atlantic Ocean. Marine Micropaleontology 1, 119–194.

Heirtzler, J.R., Bolli, H.M., Davies, T.A., Saunders, J.B., Sclater, J.G., 1977. Indian Ocean Geology and biostratigraphy. Washington, D.C.

1010 Henderiks, J., Pagani, M., 2008. Coccolithophore cell size and the Paleogene decline in atmospheric CO_2.
1011 Earth and Planetary Science Letters 269, 576–584.
1012 Huber, B.T., 1991. Paleogene and early Neogene planktonic foraminifer biostratigraphy of Sites 738 and 744,
1013 Kerguelen Plateau (southern Indian Ocean). In: Barron, J., Larsen, B., et al. (Eds.), Proceedings of the
1014 Ocean Drilling Program, Scientific Results, Volume 119: College Station, TX, Ocean Drilling Program.
1015 p. 427–449.
1016 Hutchinson, D.K., Coxall, H.K., Lunt, D.J., Steinthorsdottir, M., de Boer, A.M., Baatsen, M., von der Heydt,
1017 A., Huber, M., Kennedy-Asser, A.T., Kunzmann, L., Ladant, J.B., Lear, C.H., Moraweck, K., Pearson,
1018 P.N., Piga, E., Pound, M.J., Salzmann, U., Scher, H.D., Sijp, W.P., Śliwińska, K.K., Wilson, P.A., Zhang,
1019 Z., 2021. The Eocene–Oligocene transition: a review of marine and terrestrial proxy data, models and
1020 model–data comparisons. Climate of the Past 17, 269–315.
1021 Hyland, E., Murphy, B.H., Varela, P., Marks, K., Colwell, L., Tori, F., Monechi, S., Cleaveland, L., Brinkhuis,
1022 H., Van Mourik, C.A., Coccioni, R., Bice, D.M., Montanari, A., 2009. Integrated stratigraphic and
1023 astrochronologic calibration of the Eocene-Oligocene transition in the Monte Cagnero section
1024 (northeastern Apennines, Italy): A potential parastratotype for the Massignano global stratotype section
1025 and point (GSSP). In: Koeberl, C., Montanari, A. (Eds.), The Late Eocene Eart Hothouse, Icehouse, and
1026 Impacts. The Geological Society of America Special Paper 452, p. 303–322.
1027 Jones, A.P., Dunkley Jones, T., Coxall, H.K., Pearson, P.N., Nala, D., Hoggett, M., 2019. Low-Latitude
1028 Calcareous Nannofossil Response in the Indo-Pacific Warm Pool Across the Eocene-Oligocene
1029 Transition of Java, Indonesia. Paleoceanography and Paleoclimatology 34, 1833–1847.
1030 Kalb, A.L., Bralower, T.J., 2012. Nannoplankton origination events and environmental changes in the late
1031 Paleocene and early Eocene. Marine Micropaleontology 92–93, 1–15.
1032 Katz, M.E., Miller, K.G., Wright, J.D., Wade, B.S., Browning, J. V., Cramer, B.S., Rosenthal, Y., 2008.
1033 Stepwise transition from the Eocene greenhouse to the Oligocene icehouse. Nature Geoscience 1, 329–
1034 333.
1035 Kelly, D.C., Bralower, T.J., Zachos, J.C., Silva, I.P., Thomas, E., 1996. Rapid diversification of planktonic
1036 foraminifera in the tropical Pacific (ODP Site 865) during the late Paleocene thermal maximum. Geology
1037 24, 423–426.
1038 Kennett, J.P., 1977. Cenozoic evolution of Antarctic glaciation, the circum-Antarctic Ocean, and their impact

on global paleoceanography. Journal of Geophysical Research 82, 3843–3859.

Kleijne, A., 1991. Holococcolithophorids from the Indian Ocean, Red Sea, Mediterranean Sea and North Atlantic Ocean. Marine Micropaleontology 17, 1–76.

Langer, G., Geisen, M., Baumann, K.H., Kläs, J., Riebesell, U., Thoms, S., Young, J.R., 2006. Species-specific responses of calcifying algae to changing seawater carbonate chemistry. Geochemistry, Geophysics, Geosystems 7, 1–12.

Lear, C.H., Bailey, T.R., Pearson, P.N., Coxall, H.K., Rosenthal, Y., 2008. Cooling and ice growth across the Eocene-Oligocene transition. Geology 36, 251–254.

Lear, C.H., Lunt, D.J., 2016. How Antarctica got its ice. Science 352, 34–35.

Liu, Z., Tuo, S., Zhao, Q., Cheng, X., Huang, W., 2004. Deep-water earliest Oligocene glacial maximum (EOGM) in South Atlantic. Chinese Science Bulletin 49, 2190–2197.

López-Quirós, A., Escutia, C., Etourneau, J., Rodríguez-Tovar, F.J., Roignant, S., Lobo, F.J., Thompson, N., Bijl, P.K., Bohoyo, F., Salzmann, U., Evangelinos, D., Salabarnada, A., Hoem, F.S., Sicre, M.A., 2021. Eocene-Oligocene paleoenvironmental changes in the South Orkney Microcontinent (Antarctica) linked to the opening of Powell Basin. Global and Planetary Change 204, 103581.

Lyle, M.W., Wilson, P.A., Janecek, T.R., 2002. Leg 199 Summary. Proceedings of the Ocean Drilling Program, Initial Reports, College Station, TX (Ocean Drilling Program) 199, 1–87.

Marino, M., Flores, J.A., 2002. Middle Eocene to early Oligocene calcareous nannofossil stratigraphy at Leg 177 Site 1090. Marine Micropaleontology 45, 383–398.

Martini, E., 1971. Standard Tertiary and Quaternary calcareous nannoplankton zonation. In: Farinacci, A. (Ed.), Proceedings of the 2nd International Conference on Planktonic Microfossils. Edizioni Tecnoscienza, Rome, p. 739–785.

Merico, A., Tyrrell, T., Wilson, P.A., 2008. Eocene/Oligocene ocean de-acidification linked to Antarctic glaciation by sea-level fall. Nature 452, 979–982.

Monechi, S., Buccianti, A., Gardin, S., 2000. Biotic signals from nannoflora across the iridium anomaly in the upper Eocene of the Massignano section: evidence from statistical analysis. Marine Micropaleontology 39, 219–237.

Moore, J.C., Wade, B.S., Westerhold, T., Erhardt, A.M., Coxall, H.K., Baldauf, J., Wagner, M., 2014. Equatorial Pacific productivity changes near the Eocene-Oligocene boundary. Paleoceanography 29,

825–844.

Moran, M.J.J., Watkins, D.K.K., 1988. Oligocene Calcareous-Nannofossil Biostratigraphy from Leg 101, Site 628, Little Bahama Bank Slope. Proceedings of the Ocean Drilling Program, 101 Scientific Results 101, 87–103.

Morkhoven, F., Berggren, W.A., Edwards, A.S., Oertli, H.J., 1986. Cenozoic cosmopolitan deep-water benthic foraminifera., Bulletin des centres de recherches Exploration-production Elf-Aquitaine: Mémoire 11.

Newsam, C., Bown, P.R., Wade, B.S., Jones, H.L., 2017. Muted calcareous nannoplankton response at the Middle/Late Eocene Turnover event in the western North Atlantic Ocean. Newsletters on Stratigraphy 50, 297–309.

Nocchi, M., Parisi, G., Monaco, P., Monechi, S., Madile, M., 1988. Eocene and early Oligocene micropaleontology and paleoenvironments in SE Umbria, Italy. Palaeogeography, Palaeoclimatology, Palaeoecology 67, 181–244.

Nocchi, M., Parisi, G., Monaco, P., Monechi, S., Madile, M., Napoleone, G., Ripepe, M., Orlando, M., Premoli Silva, I., Bice, D.M., 1986. The Eocene-Oligocene Boundary in the Umbrian Pelagic Sequences, Italy. In: Developments in Palaeontology and Stratigraphy. Elsevier, Amsterdam, p. 25–40.

Nomura, R., 1991. Oligocene to Pleistocene benthic foraminifer assemblages at Sites 754 and 756, eastern Indian Ocean. Proc., scientific results, ODP, Leg 121, Broken Ridge and Ninetyeast Ridge 121, 31–75.

Norris, R.D., Wilson, P.A., Blum, P., the Expedition 342, 2014. Proceedings. IODP, 342: College Station, TX (Integrated Ocean Drilling Program).

Okada, H., Bukry, D., 1980. Supplementary modification and introduction of code numbers to the low-latitude coccolith biostratigraphic zonation. Marine Micropaleontology 5, 321–325.

Pälike, H., Lyle, M.W., Nishi, H., Raffi, I., Ridgwell, A., Gamage, K., Klaus, A., Acton, G., Anderson, L., Backman, J., Baldauf, J., Beltran, C., Bohaty, S.M., Bown, P.R., Busch, W., Channell, J.E.T., Chun, C.O.J., Delaney, M.L., Dewangan, P., Dunkley Jones, T., Edgar, K.M., Evans, H., Fitch, P., Foster, G.L., Gussone, N., Hasegawa, H., Hathorne, E.C., Hayashi, H., Herrle, J.O., Holbourn, A.E., Hovan, S., Hyeong, K., Iijima, K., Ito, T., Kamikuri, S.I., Kimoto, K., Kuroda, J., Leon-Rodriguez, L., Malinverno, A., Moore, T.C., Murphy, B.H., Murphy, D.P., Nakamura, H., Ogane, K., Ohneiser, C., Richter, C., Robinson, R., Rohling, E.J., Romero, O., Sawada, K., Scher, H.D., Schneider, L., Sluijs, A., Takata, H., Tian, J., Tsujimoto, A., Wade, B.S., Westerhold, T., Wilkens, R., Williams, T., Wilson, P.A., Yamamoto,

Y., Yamamoto, S., Yamazaki, T., Zeebe, R.E., 2012. A Cenozoic record of the equatorial Pacific carbonate compensation depth. Nature 488, 609–614.

Pälike, H., Norris, R.D., Herrle, J.O., Wilson, P.A., Coxall, H.K., Lear, C.H., Shackleton, N.J., Tripati, A.K., Wade, B.S., 2006. The heartbeat of the Oligocene climate system. Science 314, 1894–1898.

Pearson, P.N., McMillan, I.K., Wade, B.S., Dunkley Jones, T., Coxall, H.K., Bown, P.R., Lear, C.H., 2008. Extinction and environmental change across the Eocene-Oligocene boundary in Tanzania. Geology 36, 179–182.

Pearson, P.N., Olsson, R.K., Huber, B.T., Hemleben, C., Berggren, W.A., 2006. Atlas of Eocene planktonic foraminifera (No. 41). Cushman Foundation for Foraminiferal Research.

Peirce, J., Weissel, J., et al., 1989a. Leg 121 Background and objectives. Proceeding ODP, Initial Reports, 121: College Station, TX (Ocean Drilling Program).

Peirce, J., Weissel, J., et al., 1989b. Site 756. Proceeding ODP, Initial Reports, 121: College Station, TX (Ocean Drilling Program).

Perch-Nielsen, K., 1985. Cenozoic calcareous nannofossils. In: Bolli, H.M., Saunders, J.B., Perch-Nielsen, K. (Eds.), Plankton Stratigraphy. Cambridge University Press, Cambridge, p. 427–555.

Perch-Nielsen, K., 1986. Calcareous nannofossil events at Eocene/Oligocene boundary. In: Pomerol, C., Premoli Silva, I. (Eds.), Terminal Eocene Events. Elsevier, Amsterdam, p. 275–282.

Persico, D., Villa, G., 2004. Eocene-Oligocene calcareous nannofossils from Maud Rise and Kerguelen Plateau (Antarctica): Paleoecological and paleoceanographic implications. Marine Micropaleontology 52, 153–179.

Persico, D., Villa G., 2008. A new Eocene Chiasmolithus species: hypothetical reconstruction of its phyletic lineage. Journal of Nannoplankton Research 30, 23-33

Pospichal, J.J., 1991. Calcareous nannofossils across Cretaceous/Tertiary boundary at Site 752, eastern Indian Ocean. Proceedings of the Ocean Drilling Program, College Station, TX, 121 395–413.

Premoli Silva, I., Jenkins, D.G., 1993. Decision on the Eocene-Oligocene boundary stratotype. Episodes 16, 379–382.

Premoli Silva, I., Orlando, M., Monechi, S., Madile, M., Napoleone, G., Ripepe, M., 1988. Calcareous plankton biostratigraphy and magnetostratigraphy at the Eocene-Oligocene transition in the Gubbio area. International Subcommission on Paleogene Stratigraphy, Eocene/Oligocene Meeting, Spec. Publ., II 6,

137–161.

Raffi, I., Agnini, C., Backman, J., Catanzariti, R., Pälike, H., 2016. A Cenozoic calcareous nannofossil biozonation from low and middle latitudes: A synthesis. Journal of Nannoplankton Research 36, 121–132.

Ravizza, G., Paquay, F., 2008. Os isotope chemostratigraphy applied to organic-rich marine sediments from the Eocene-Oligocene transition on the West African margin (ODP Site 959). Paleoceanography 23, 1–11.

Reghellin, D., Coxall, H.K., Dickens, G.R., Backman, J., 2015. Carbon and oxygen isotopes of bulk carbonate in sediment deposited beneath the eastern equatorial Pacific over the last 8 million years. Paleoceanography 30, 1261–1286.

Salamy, K.A., Zachos, J.C., 1999. Latest Eocene-Early Oligocene climate change and Southern Ocean fertility: Inferences from sediment accumulation and stable isotope data. Palaeogeography, Palaeoclimatology, Palaeoecology 145, 61–77.

Sarmiento, J.L., Gruber, N., Brzezinski, M.A., Dunne, J.P., 2004. High-latitude controls of thermocline nutrients and low latitude biological productivity. Nature 427, 56–60.

Schneider, L.J., Bralower, T.J., Kump, L.R., 2011. Response of nannoplankton to early Eocene ocean destratification. Palaeogeography, Palaeoclimatology, Palaeoecology 310, 152–162.

Shannon, C.E., Weaver, W., 1949. The Mathematical Theory of Communication. University of Illinois Press, Champaign, IL.

Shaw, A.B., 1964. Adequacy of the Fossil Record. In: Time in Stratigraphy. Mc Graw-Hill, p. 105–117.

Shcherbinina, E., 2010. Response of early Paleogene nannofossils to periodically increased nutrient availability in the NE Peri-Tethys. Geophysical Research Abstracts 12, 13597.

Spofforth, D.J.A., Agnini, C., Pälike, H., Rio, D., Fornaciari, E., Giusberti, L., Luciani, V., Lanci, L., Muttoni, G., 2010. Organic carbon burial following the middle Eocene climatic optimum in the central western Tethys. Paleoceanography 25, PA3210.

Sverdrup, H.U., Johnson, M.W., Fleming, R.H.., 1942. The Oceans: their physics, chemistry, and general biology. Prentice-Hall, Inc., New York.

Toffanin, F., Agnini, C., Fornaciari, E., Rio, D., Giusberti, L., Luciani, V., Spofforth, D.J.A., Pälike, H., 2011. Changes in calcareous nannofossil assemblages during the Middle Eocene Climatic Optimum: Clues

from the central-western Tethys (Alano section, NE Italy). Marine Micropaleontology 81, 22–31.

Toffanin, F., Agnini, C., Rio, D., Acton, G., Westerhold, T., 2013. Middle eocene to early oligocene calcareous nannofossil biostratigraphy at IODP site U1333 (equatorial pacific). Micropaleontology 59, 69–82.

Tremolada, F., Bralower, T.J., 2004. Nannofossil assemblage fluctuations during the Paleocene-Eocene Thermal Maximum at Sites 213 (Indian Ocean) and 401 (North Atlantic Ocean): palaeoceanographic implications. Marine Micropaleontology 52, 107–116.

Via, R.K., Thomas, D.J., 2006. Evolution of Atlantic thermohaline circulation: Early Oligocene onset of deep-water production in the North Atlantic. Geology 34, 441–444.

Villa, G., Fioroni, C., Pea, L., Bohaty, S.M., Persico, D., 2008. Middle Eocene-late Oligocene climate variability: Calcareous nannofossil response at Kerguelen Plateau, Site 748. Marine Micropaleontology 69, 173–192.

Villa, G., Fioroni, C., Persico, D., Roberts, A.P., Florindo, F., 2014. Middle Eocene to Late Oligocene Antarctic glaciation/deglaciation and Southern Ocean productivity. Paleoceanography 29, 223–237.

Villa, G., Florindo, F., Persico, D., Lurcock, P., de Martini, A.P., Jovane, L., Fioroni, C., 2021. Integrated calcareous nannofossil and magnetostratigraphic record of ODP Site 709: Middle Eocene to late Oligocene paleoclimate and paleoceanography of the Equatorial Indian Ocean. Marine Micropaleontology 169, 102051.

Villa, G., Persico, D., 2006. Late Oligocene climatic changes: Evidence from calcareous nannofossils at Kerguelen Plateau Site 748 (Southern Ocean). In: Palaeogeography, Palaeoclimatology, Palaeoecology. Elsevier, p. 110–119.

Wade, B.S., Aljahdali, M.H., Mufrreh, Y.A., Memesh, A.M., Alsoubhi, S.A., Zalmout, I.S., 2021. Upper Eocene planktonic foraminifera from northern Saudi Arabia: Implications for stratigraphic ranges. Journal of Micropalaeontology 40, 145–161.

Wade, B.S., Bown, P.R., 2006. Calcareous nannofossils in extreme environments: the Messinian Salinity Crisis, Polemi Basin, Cyprus. Palaeogeography, Palaeoclimatology, Palaeoecology 233, 271–286.

Wade, B.S., Olsson, R.K., 2009. Investigation of pre-extinction dwarfing in Cenozoic planktonic foraminifera. Palaeogeography, Palaeoclimatology, Palaeoecology 284, 39–46.

Wade, B.S., Olsson, R.K., Pearson, P.N., Huber, B.T., Berggren, W.A., 2018. Atlas of Oligocene Planktonic Foraminifera. Cushman Foundation Special Publication 46, Washington D.C.

Wade, B.S., Pearson, P.N., 2008. Planktonic foraminiferal turnover, diversity fluctuations and geochemical signals across the Eocene/Oligocene boundary in Tanzania. Marine Micropaleontology 68, 244–255.

Wei, W., Wise, S.W., 1990. Biogeographic gradients of middle Eocene-Oligocene calcareous nannoplankton in the South Atlantic Ocean. Palaeogeography, Palaeoclimatology, Palaeoecology 79, 29–61.

Wei, W.C., Villa, G., Wise, S.W., Wuchang Wei, Villa, G., Wise, S.W., 1992. Paleoceanographic implications of Eocene-Oligocene calcareous nannofossils from Sites 711 and 748 in the Indian Ocean. Proceedings of the Ocean Drilling Program, 120 Scientific Results 120, 979–999.

Winter, A., Jordan, R.W., Roth, P.H., 1994. Biogeography of living coccolithophores in ocean waters. In: Winter, A., Siesser, W.G. (Eds.), Coccolithophores. Cambridge University Press, Cambridge, p. 161–177.

Young, J.R., 1998. Neogene. In: Bown, P. (Ed.), Calcareous Nannofossil Biostratigraphy. Kluwer Academic Publishers, p. 225–265.

Young, J.R., Geisen, M., Probert, I., 2005. A review of selected aspects of coccolithophore biology with implications for paleobiodiversity estimation. Micropaleontology 51, 267–288.

Zachos, J.C., Kump, L.R., 2005. Carbon cycle feedbacks and the initiation of Antarctic glaciation in the earliest Oligocene. Global and Planetary Change.

Zachos, J.C., Pagani, M., Sloan, L., Thomas, E., Billups, K., 2001. Trends, Global Rhythms, and Aberrations in Global Climate 65 Ma to Present. Science 292, 686–693.

Zachos, J.C., Quinn, T.M., Salamy, K.A., 1996. High-resolution (10^4 years) deep-sea foraminiferal stable isotope records of the Eocene-Oligocene climate transition. Paleoceanography 11, 251–266.

Zachos, J.C., Rea, D.K., Seto, K., Nomura, R., Niitsuma, N., 1992. Paleogene and Early Neogene Deep Water Paleoceanography of the Indian Ocean as Determined from Benthic Foraminifer Stable Carbon and Oxygen Isotope Records. In: Duncan, R.A., Rea, D.K., Kidd, R.B., Rad, U. von, Weissel, J.K. (Eds.), Synthesis of Results from Scientific Drilling in the Indian Ocean, Volume 70. American Geophysical Union, p. 351–385.

9 FIGURES, 2 TABLES, 4 PLATES, 1 APPENDIX

Fig. 1. Location of ODP Site 756 shown on a paleomap (Mercator projection) at 34 Ma, reconstruction from http://www.odsn.de/. The approximate pathway of shallow-intermediate and deep waters masses during the EOT, as inferred from Zachos et al. (1992), is also shown. IDW = Indian Deep Water; AAIW=Antarctic Intermediate Water; AABW = Antarctic Bottom Water; TISW = Tethyan-Indian saline water

Fig. 2. Biostratigraphic classification of the study succession at Hole 756C based on calcareous nannofossils. The adopted schemes are those of Okada and Bukry 1980 (CP), Martini 1971 (NP) and Agnini et al. 2014 (CNE). Biohorizons are also indicated and defined as B (Base), Bc (Base common), T (Top), Tc (Top common). Biochronological estimations calibrated to the GTS12 are provided. Chronostratigraphy is also plotted along depth (mbsf).

Fig. 3. Semi-quantitative (n/mm^2) and relative (%) abundance patterns of biostratigraphically significant taxa from Hole 756C are plotted versus depth (mbsf), lithology, calcareous nannofossil biostratigraphy (NP, Martini 1971; CP, Okada and Bukry 1980; CN, Agnini et al. 2014) and chronostratigraphy. Events are termed as: B = Base, Bc= Base common and continuous, T = Top, Tc= Top common and continuous. The EOGM (light blue bar) and EOT (grey bar) are also reported and refer to the oxygen stable isotopes results from paragraph 3.2.

Fig. 4. $\delta^{18}O$ (‰), $CaCO_3$ (%), $\delta^{13}C$ (‰), H index, cumulative percentage of calcareous nannofossils genera from ODP Hole 756C plotted against depth (mbsf), lithology, calcareous nannofossil biozones (NP, Martini 1971; CP, Okada and Bukry 1980; CN, Agnini et al. 2014) and chronostratigraphy. Benthic foraminiferal stable isotopes were analyzed on *Cibicidoides havanensis* and *C. mundulus*. We highlight the EOT-shift as well as the two $\delta^{18}O$ steps (horizontal grey bar) using the terminology of Hutchinson et al (2021). The early Oligocene $\delta^{18}O$ maximum, referred to as the Early Oligocene Glacial Maximum (EOGM) is denoted by a light blue bar.

Fig. 5. Nannofossil genera (%) are compared along with geochemical data ($\delta^{18}O$‰, $CaCO_3$%, $\delta^{13}C$ ‰) from Hole 756C. Data are plotted against depth (mbsf), lithology, calcareous nannofossils biostratigraphy (NP, Martini 1971; CP, Okada and Bukry 1980; CN, Agnini et al. 2014) and chronostratigraphy. The horizontal grey bar indicates the two positive steps in $\delta^{18}O$ recognized at the EOT and the light blue bar indicates the maximum values of $\delta^{18}O$ (EOGM).

Fig. 6. Age-depth plot and sedimentation rates across the E-O transition, Hole 756C. Tie-points ages are based on calcareous nannofossil datums (blue squares), planktonic foraminifera *Hantkenina* spp. extinction (green diamond) and EOIS (magenta circle). The position of the T of *G. index* and pseudohastigerinid dwarfing event (green diamonds) are also reported in the plot but they were not included in the age-model. Symbols are shown with error bars in the depth domain, representing the lowermost and uppermost depths of biohorizons. See Table 1 for data points. EOGM, EOB and EOT are also shown.

Fig. 7. Screen plot from PCA, showing the relative importance of the principal components (PCs) in terms of explained variance.

Fig. 8. Results of principal component analysis (PCA; correlation matrix) based on calcareous nannofossil assemblage from ODP Site 756. (A) PCA biplot showing PC1 (interpreted as sea surface temperature SST) and PC2 (interpreted as trophic conditions). Samples are divided in: "Late Eocene", "EOT", "EOGM" and "Oligocene" based on the position of the isotopic shifts. (B) Principal component scores and loadings of calcareous nannofossil taxa on the two principal components. Data are plotted against depth (mbsf), calcareous nannofossil biozones (NP, Martini 1971; CP, Okada and Bukry 1980; CN, Agnini et al. 2014) and chronostratigraphy.

Fig. 9. Relative (%) abundance of reticulofenestrids at ODP Hole 756C are plotted against stable oxygen and carbon isotopes ($\delta^{18}O$; $\delta^{13}C$) from bulk and benthic foraminifera (*C. mundulus* and *C. havanensis*) and bulk carbonate content ($CaCO_3$%). Principal component scores (PC1 and PC2) are also reported as indices, respectively, of temperature and paleoproductivity. Data are plotted against depth (mbsf), lithology, calcareous nannofossils biozones (NP, Martini, 1971; CP, Okada and Bukry, 1980; CN, Agnini et al., 2014) and chronostratigraphy. The horizontal grey bar indicates the two positive steps in $\delta^{18}O$ recognized at the EOT (Step 1 and EOIS) and the light blue bar indicates the maximum values of $\delta^{18}O$ (EOGM). The base of the EOT is marked by the extinction of *D. saipanensis* (Hutchinson et al. 2021).

Table 1. Position (in mbsf) of calcareous plankton (calcareous nannofossils, planktonic foraminifera *Hantkenina, P. micra* and *G. index*) and geochemical events at ODP Hole 756C. The grey bars represent the tie-points (in bold) used in the construction of the age model. The ages of tie-points were assigned using the Geological Time Scale calibration ages (GTS12, Gradstein et al. 2012). Other investigated bioevents are calculated by applying linear interpolation between tie-points, assuming constant sedimentation rates. Datum type is also reported: CN (calcareous nannofossil), PF (planktonic foraminifera) and IS (oxygen isotopes)

Table 2. Synthesis of calcareous nannofossil paleoecological affinities based on previous literature and on this study.

Plate 1. LM (magnification 1250x) microphotographs of selected calcareous nannofossil taxa from ODP Hole 756C. Scale bar = 5 μm. Photos **1-18** are in crossed nicols; **19, 20** in parallel light. **1, 2.** *Reticulofenestra umbilicus*. Samples 756C-6X-1W, 140 cm (121.60 mbsf); 756C-7X-2W, 140 cm (132.70 mbsf). **3, 4.** *Reticulofenestra daviesii*, Sample 756C-6X-5W, 80 cm (127.00 mbsf). **5.** *Cyclicargolithus floridanus*. Sample 756C-5X-7W, 140 cm (117.01 mbsf). **6,7.** *Dictyococcites bisectus*. Sample 756C-6X-1W, 20 cm (120.40 mbsf). **8, 9.** *Dictyococcites* spp. Samples 756C-6X-1W, 140 cm (121.60 mbsf); 756C-6X-4W, 80 cm (125.50 mbsf). **10.** *Dictyococcites hesslandii*. Sample 756C-6X-4W, 60 cm (125.30 mbsf). **11.** *Coccolithus eopelagicus*. Sample 756C-7X-2W, 140 cm (132.70 mbsf). **12.** *Ericsonia formosa*. Sample 756C-7X-1W, 80 cm (130.60 mbsf). **13, 14.** *Clausicoccus subdistichus*. Sample 756C-6X-5W, 80 cm (127.00 mbsf). **15, 16.** *Chiasmolithus altus*. Samples 756C-5X-7W, 140 cm (117.01 mbsf); 756C-6X-1W, 20 cm (120.40 mbsf). **17.** *Chiasmolithus oamaruensis*. Sample 756C-6X-4W, 90 cm (125.60 mbsf). **18, 19.** *Helicosphaera compacta*. Sample 756C-5X-8W, 20 cm (117.31 mbsf). **20.** *Discoaster barbadiensis*. Sample 756C-7X-2W, 60 cm (131.90 mbsf).

Plate 2. LM (magnification 1250x) microphotographs of selected calcareous nannofossil taxa from ODP Hole 756C. Scale bar = 5 μm. All photos are in crossed nicols except for **4, 15, 16** which are in parallel light. **1, 2.** *Chiasmolithus altus*. Samples 756C-6X-1W, 140 cm (121.60 mbsf), 756C-6X-4W, 80 cm (125.50 mbsf). 3, 4. *Chiasmolithus* cf. *C. oamaruensis*. Sample 756C-6X- 4W, 80 cm (125.50 mbsf). **5.** *Bramletteius serraculoides*. Sample 756C-6X-4W, 80 cm (125.50 mbsf). **6, 7.** *Isthmolithus recurvus*. Samples 756C-6X-5W, 80 cm (127.00 mbsf); 756C-7X-2W, 140 cm (132.70 mbsf). **8, 9.** *Lanternithus minutus*. Samples 756C-6X-4W, 129 cm (125.99 mbsf); 756C-6X-5W, 70 cm (126.90 mbsf). **10, 12.** *Zygrhablithus bijugatus*. Sample 756C-6X-3W, 50 cm (123.70 mbsf). **11.** *Zygrhablithus bijugatus* base. Sample 756C-6X-3W, 50 cm (123.70 mbsf). **13.** *Thoracosphaera* spp. Sample 756C-6X-1W, 20 cm (120.40 mbsf). **14.** *Pontosphaera* spp. Sample 756C-7X-2W, 140 cm (132.70 mbsf). **15.** *Discoaster* cf. *D. deflandrei*. Sample 756C-6X-4W, 129 cm (125.99 mbsf). **16.** *Discoaster tanii*, 756C-6X-5W, 80 cm (127.00 mbsf). **17.** *Reticulofenestra* spp. Sample 756C-5X-5W, 60 cm (114.06 mbsf). **18.** *Reticulofenestra dictyoda*. Sample 756C-7X-2W, 19 cm (131.49 mbsf). **19.** *Blackites* cf. *B. singulus*. Sample 756C-6X-1W, 140 cm (121.60 mbsf). **20.** *Umbilicosphaera* spp. Sample 756C-6X-3W, 69 cm (123.89 mbsf).

Plate 3. LM (magnification 1250x) microphotographs of selected calcareous nannofossil taxa from ODP Hole 756. Scale bar = 5 μm. Photos **1-5** and **19, 20** are in parallel light; photos **6-18** are in crossed nicols. **1.** *Discoaster tanii nodifer*. Sample 756C-6X-5W, 80 cm (127.00 mbsf). **2.** *Discoaster barbadiensis*. Sample 756C-7X-2W, 19 cm (131.49 mbsf). **3-5.** *Discoaster saipanensis*. Sample 756C-7X-2W, 19 cm (131.49 mbsf). **6.** *Sphenolithus moriformis* gr. Sample 756C-7X-2W, 80 cm (132.10 mbsf). **7, 8.** *Sphenolithus akropodus* morphotype A (45°, 0°). Sample 756C-6X-1W, 20 cm (120.40 mbsf). **9, 10**. *Sphenolithus akropodus* morphotype B (45°, 0°). Sample 756C-6X-1W, 20 cm (120.40 mbsf). **11-14.** *Sphenolithus predistentus* (45°, 0°). Samples 756C-5X-6W, 0 cm 114.28 mbsf); 756C-5X-7W, 140 cm (117.01 mbsf). **15, 16.** *Sphenolithus distentus* (45°, 0°). Sample 756C-5X-6W, 0 cm (114.28 mbsf). **17.** *Reticulofenestra umbilicus*. Sample 756C-6X-1W, 140 cm (121.60 mbsf). **18, 19.** *Chiasmolithus altus*. Sample 756C-6X-1W, 140 cm (121.60 mbsf). **20.** *Discoaster* cf. *D. deflandrei*. Sample 756C-5X-7W, 140 cm (117.01 mbsf).

Plate 4. SEM images of selected Eocene-Oligocene foraminifera from Hole 756C. Scale bars: **21**, 400 μm; **22** and **23**, 300 μm; **1**, **3**, **5**, **6**, **8**, **9**, **19**, **20**, 100 μm; **2** and **10-18**, 50 μm; **24**, 40 μm; **4** and **7**, 20 μm.
1. *Hantkenina alabamensis* with post depositional borings. Sample 756C-6X-5, 20-22 cm. **2.** *H. alabamensis* close-up**,** showing surface striations and dissolution. Sample 756C-6X-5, 20-22 cm. **3.** *H. alabamensis* test fragment, strongly dissolved, peeled and partially recrystallized. Sample 756C-6X-3,129.5-131.5 cm. **4.** *H. alabamensis* close-up. Sample 756C-6X-3,129.5-131.5 cm. **5.** *H. alabamensis*. Sample 756C-6X-4, 10 cm. **6.** *Globigerinahteka index*. Sample 756C-7X-1, 115 cm. **7.** *G. index* zoom in showing recrystallized test. Sample 756C-7X-1, 115 cm. **8.** *Turborotalia ampliapertura*. Sample 756C-5X-8, 100-102 cm. **9.** *T. increbescens*. Sample 756C-6X-4,10 cm. **10.** *Chiloguembelina ototara*. Sample 756C-5X-8, 40-42 cm. **11**. *C. ototara*. Sample 756C-6X-2, 131.5-133.5 cm. **12.** *Tenuitella gemma*. Sample 756C-5X-8, 40-42 cm. **13, 14.** *Tenuitella gemma*. Sample 756C-6X-2, 131.5-133.5 cm. **15-17.** *Pseudohastigerina naguewichiensis*. Sample 756C-6X-2, 131.5-133.5 cm. **18.** *P. micra* or *P. naguewichiensis*. Sample 756C-6X-2, 131.5-133.5 cm. **19, 20.** *P. micra*? Sample 756C-6X-2, 131.5-133.5 cm. **21.** *Cibicidoides* cf. *havanensis*. Sample 756C-7X-4, 110 cm. **22, 23.** *Cibicidoides mundulus?* Sample 756C-7X-4, 110 cm. **24.** Zoom in of *Cibicidoides mundulus?* wall showing the relatively good preservation. Sample 756C-7X-4, 110 cm.

Appendix. Taxa encountered and cited in this study are listed in alphabetic order.

Figure 1

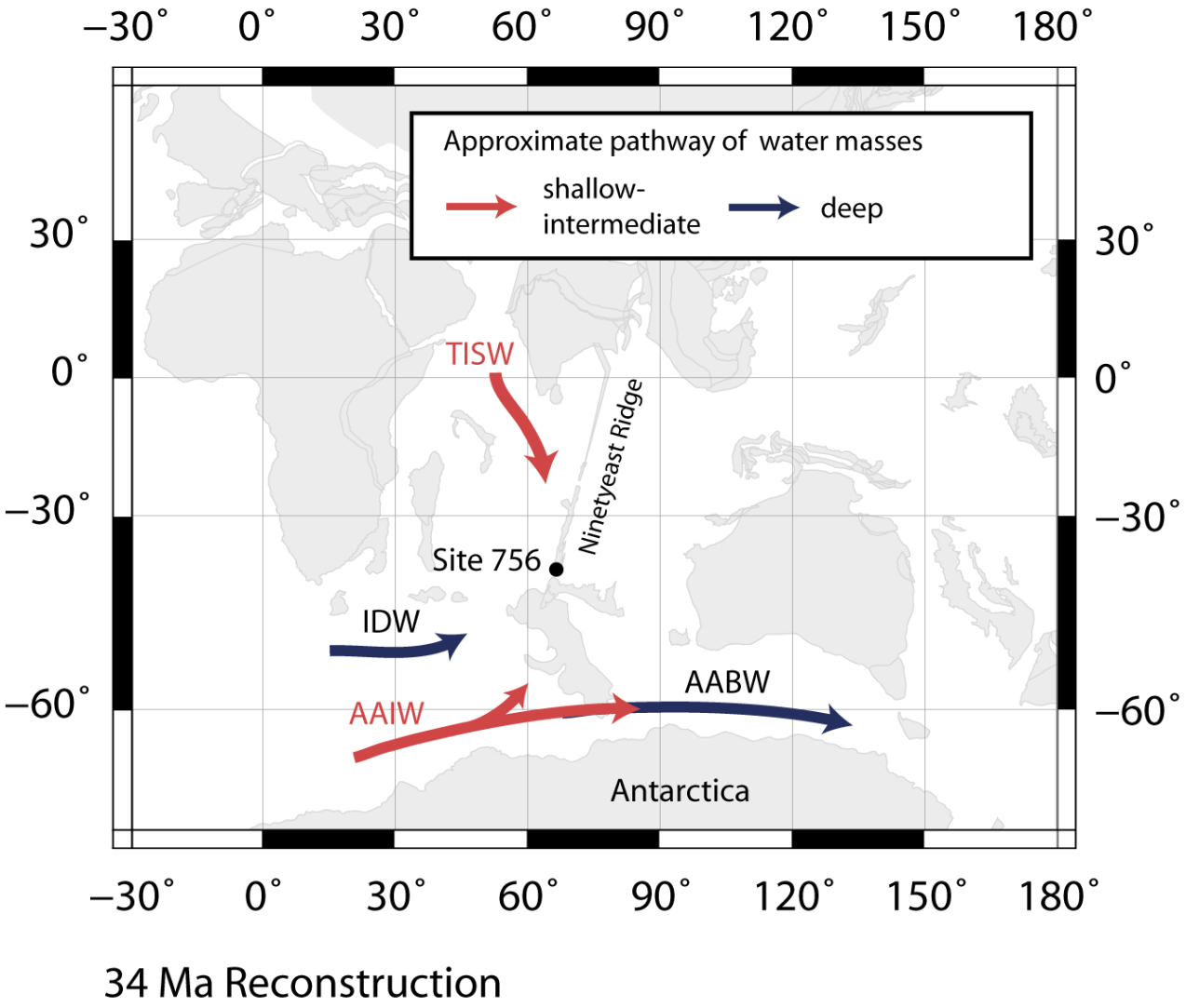
−30°
0°
30°
60°
90°
120°
150°
180°
Approximate pathway of water masses
shallow-intermediate
deep
30°
0°
−30°
−60°
TISW
Ninetyeast Ridge
Site 756
IDW
AABW
AAIW
Antarctica
34 Ma Reconstruction

Figure 2

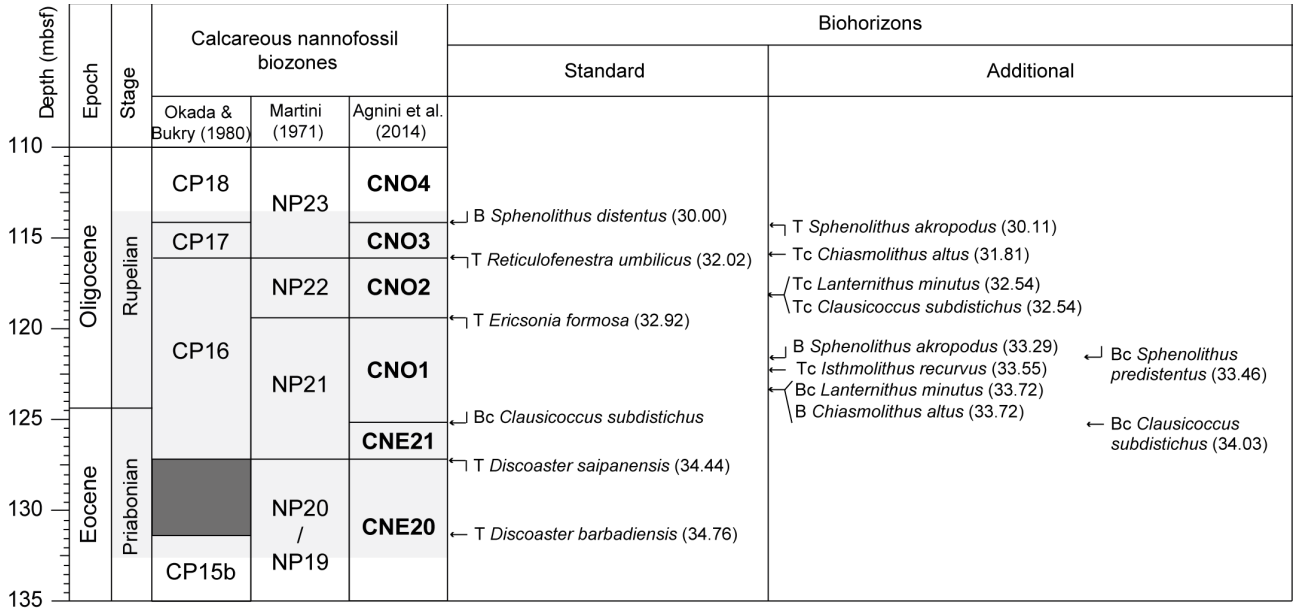
Depth (mbsf)
Epoch
Stage
Calcareous nannofossil biozones
Okada & Bukry (1980)
Martini (1971)
Agnini et al. (2014)
Biohorizons
Standard
Additional
110
115
120
125
130
135
Oligocene
Eocene
Rupelian
Priabonian
CP18
CP17
CP16
CP15b
NP23
NP22
NP21
NP20 / NP19
CNO4
CNO3
CNO2
CNO1
CNE21
CNE20
B Sphenolithus distentus (30.00)
T Reticulofenestra umbilicus (32.02)
T Ericsonia formosa (32.92)
Bc Clausicoccus subdistichus
T Discoaster saipanensis (34.44)
T Discoaster barbadiensis (34.76)
T Sphenolithus akropodus (30.11)
Tc Chiasmolithus altus (31.81)
Tc Lanternithus minutus (32.54)
Tc Clausicoccus subdistichus (32.54)
B Sphenolithus akropodus (33.29)
Tc Isthmolithus recurvus (33.55)
Bc Lanternithus minutus (33.72)
B Chiasmolithus altus (33.72)
Bc Sphenolithus predistentus (33.46)
Bc Clausicoccus subdistichus (34.03)

1394 Figure 3

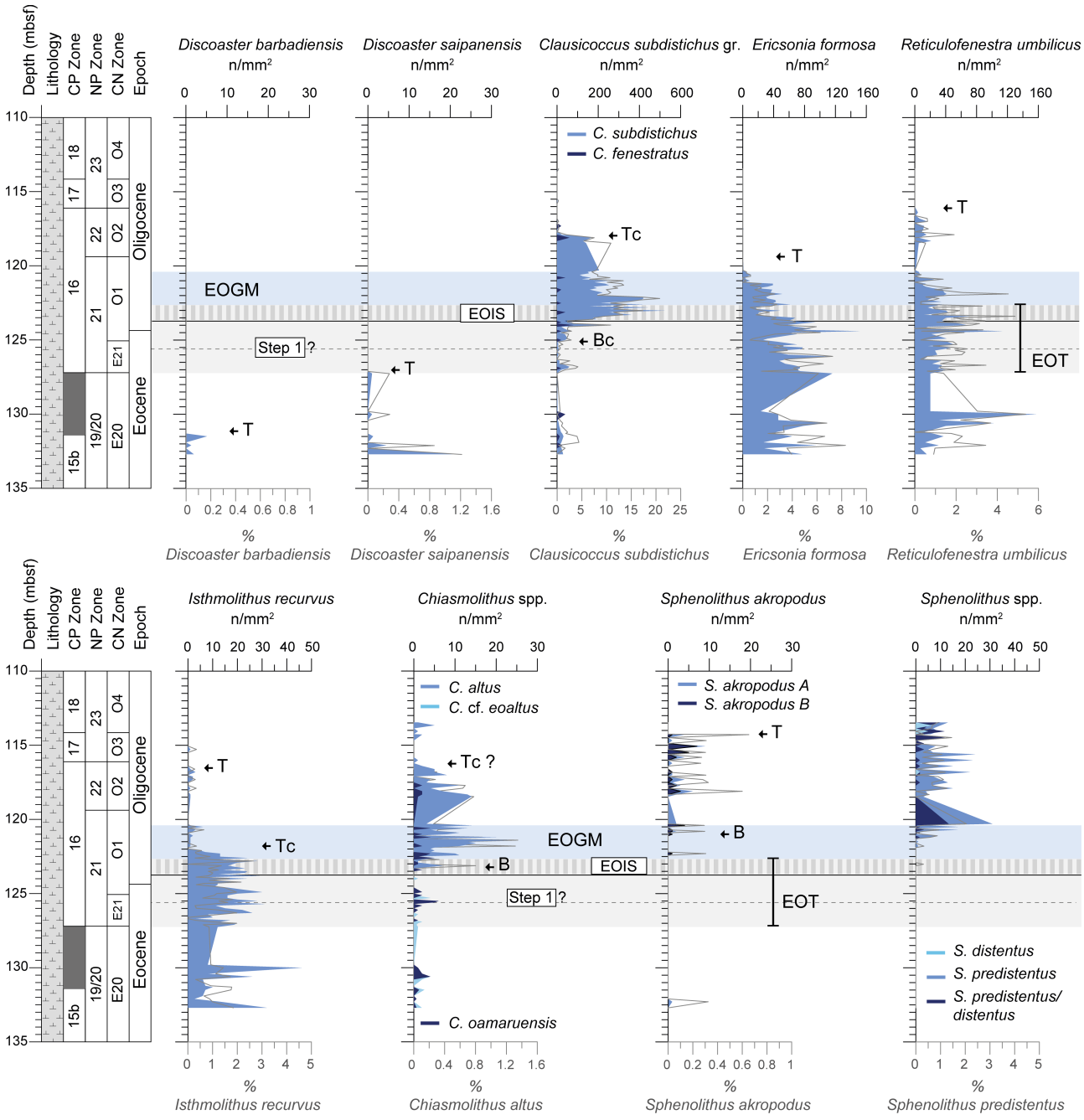

1395

1396

1397

1398

1399

1400

1401

1402

1403

Figure 4

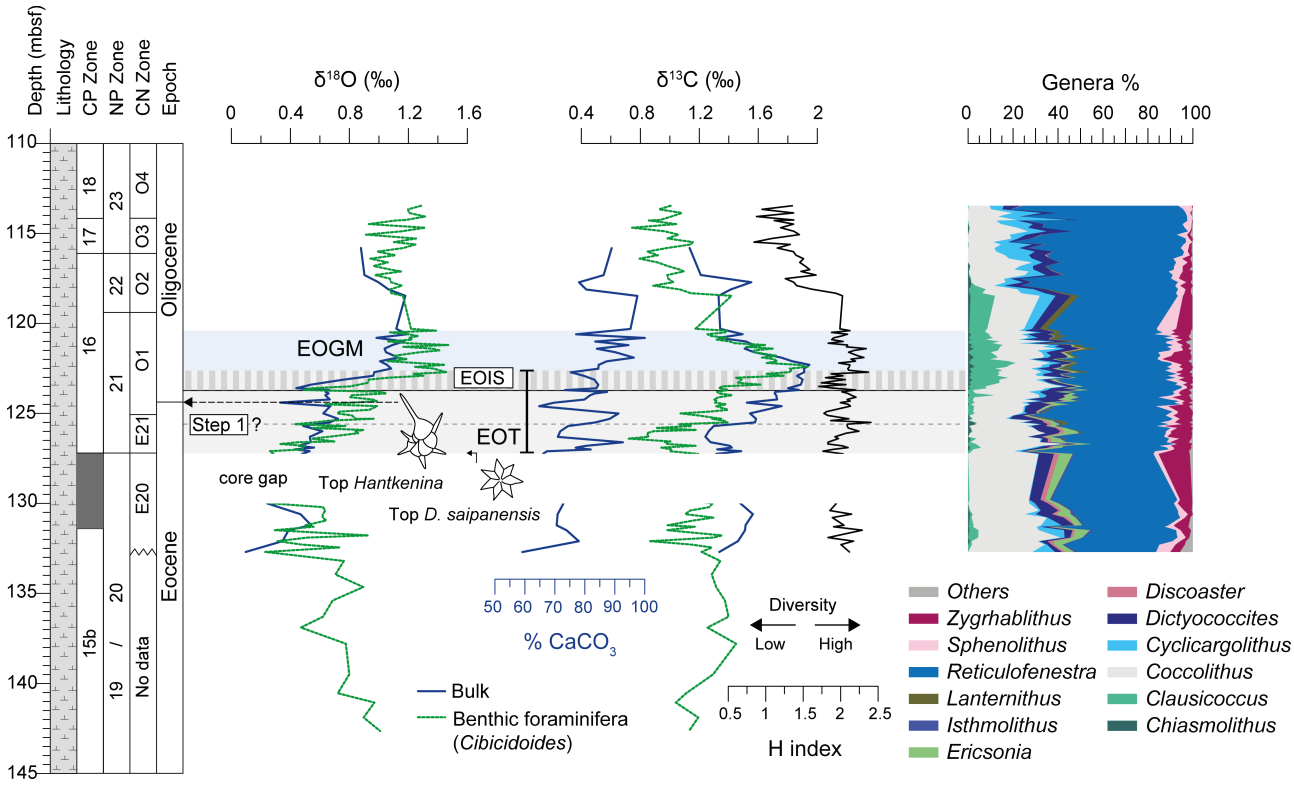
Depth (mbsf)
Lithology
CP Zone
NP Zone
CN Zone
Epoch
δ18O (‰)
δ13C (‰)
Genera %
EOGM
EOIS
EOT
Step 1 ?
core gap
Top Hantkenina
Top D. saipanensis
% CaCO3
Bulk
Benthic foraminifera (Cibicidoides)
Diversity
Low
High
H index
Others
Zygrhablithus
Sphenolithus
Reticulofenestra
Lanternithus
Isthmolithus
Ericsonia
Discoaster
Dictyococcites
Cyclicargolithus
Coccolithus
Clausicoccus
Chiasmolithus
Oligocene
Eocene
No data

Figure 5

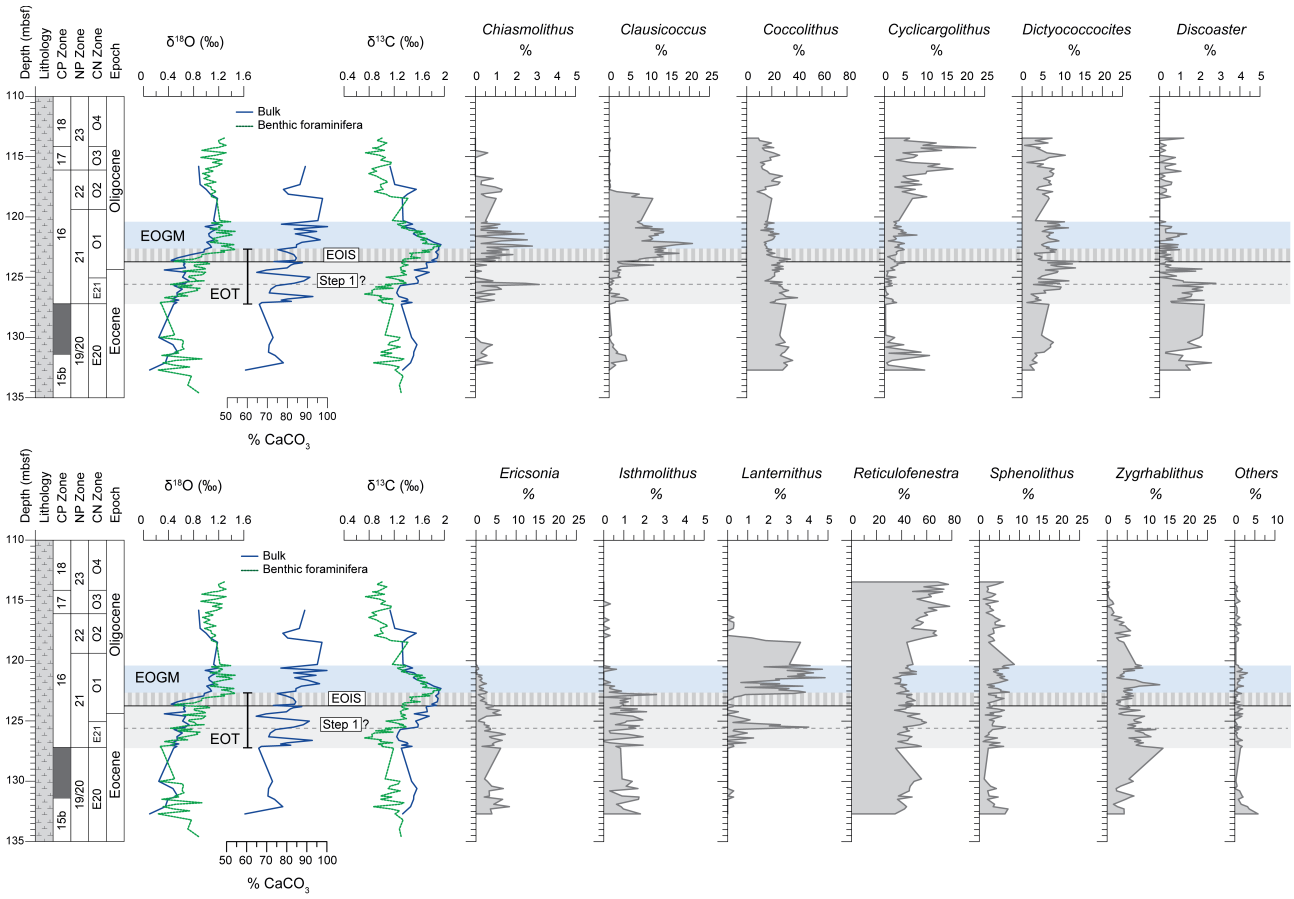
Depth (mbsf)
Lithology
CP Zone
NP Zone
CN Zone
Epoch
δ18O (‰)
δ13C (‰)
Bulk
Benthic foraminifera
EOGM
EOIS
Step 1?
EOT
% CaCO3
Chiasmolithus %
Clausicoccus %
Coccolithus %
Cyclicargolithus %
Dictyococcocites %
Discoaster %
Ericsonia %
Isthmolithus %
Lanternithus %
Reticulofenestra %
Sphenolithus %
Zygrhablithus %
Others %
Oligocene
Eocene

Figure 6

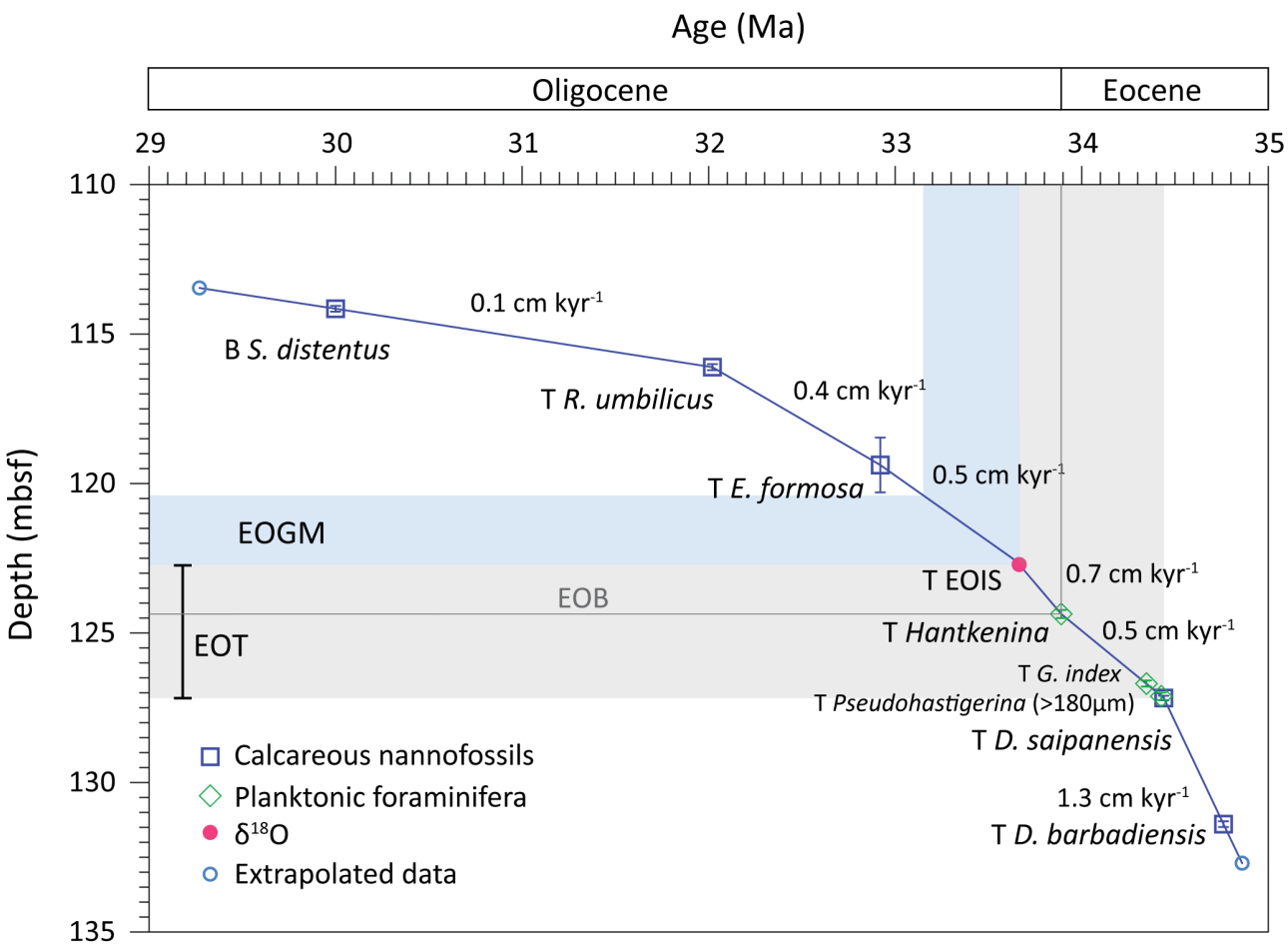
Age (Ma)
Oligocene
Eocene
29
30
31
32
33
34
35
110
115
120
125
130
135
Depth (mbsf)
0.1 cm kyr-1
B S. distentus
T R. umbilicus
0.4 cm kyr-1
T E. formosa
0.5 cm kyr-1
EOGM
T EOIS
0.7 cm kyr-1
EOB
T Hantkenina
0.5 cm kyr-1
EOT
T G. index
T Pseudohastigerina (>180µm)
T D. saipanensis
1.3 cm kyr-1
T D. barbadiensis
Calcareous nannofossils
Planktonic foraminifera
δ18O
Extrapolated data

Figure 7

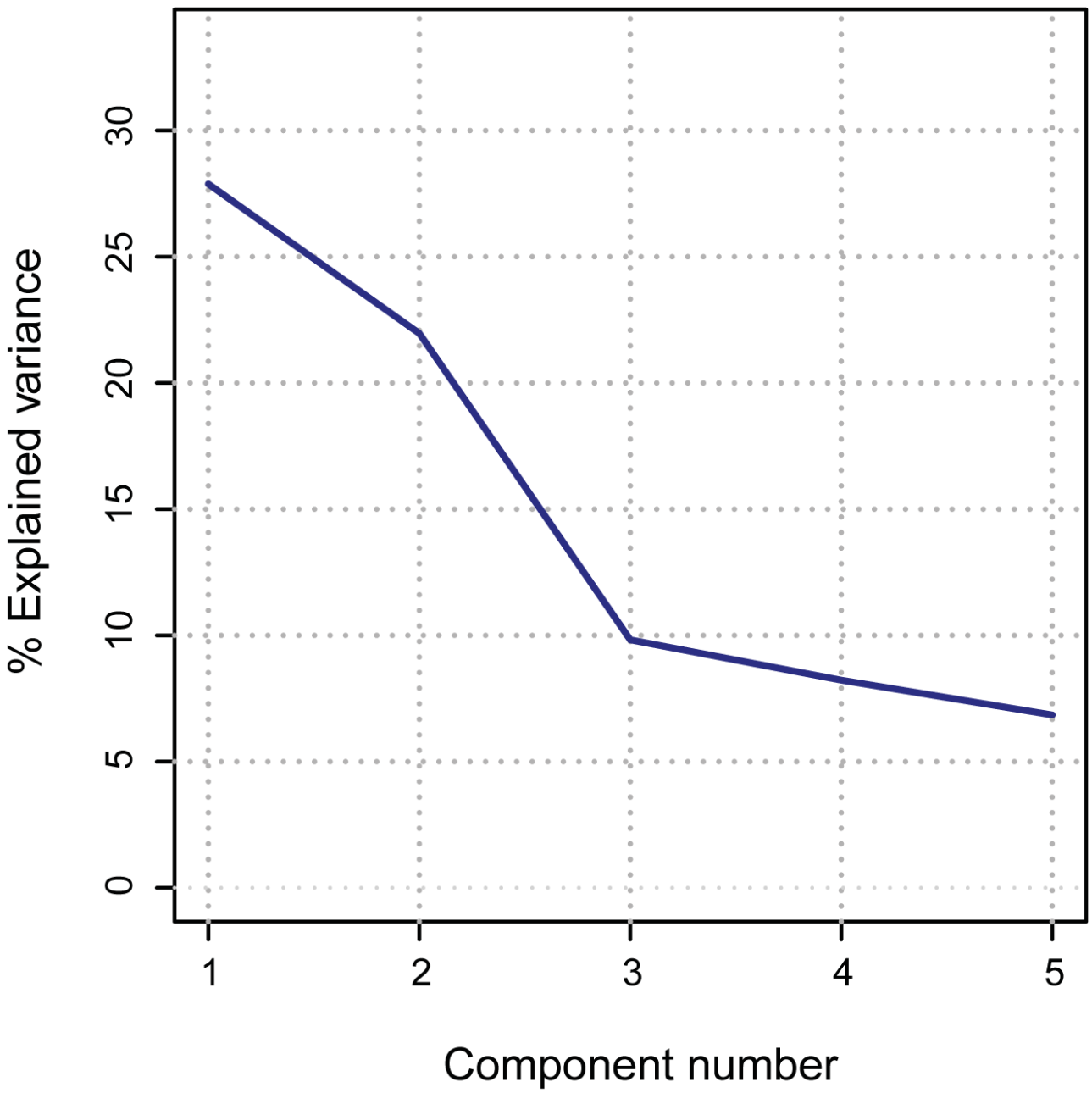

Figure 8

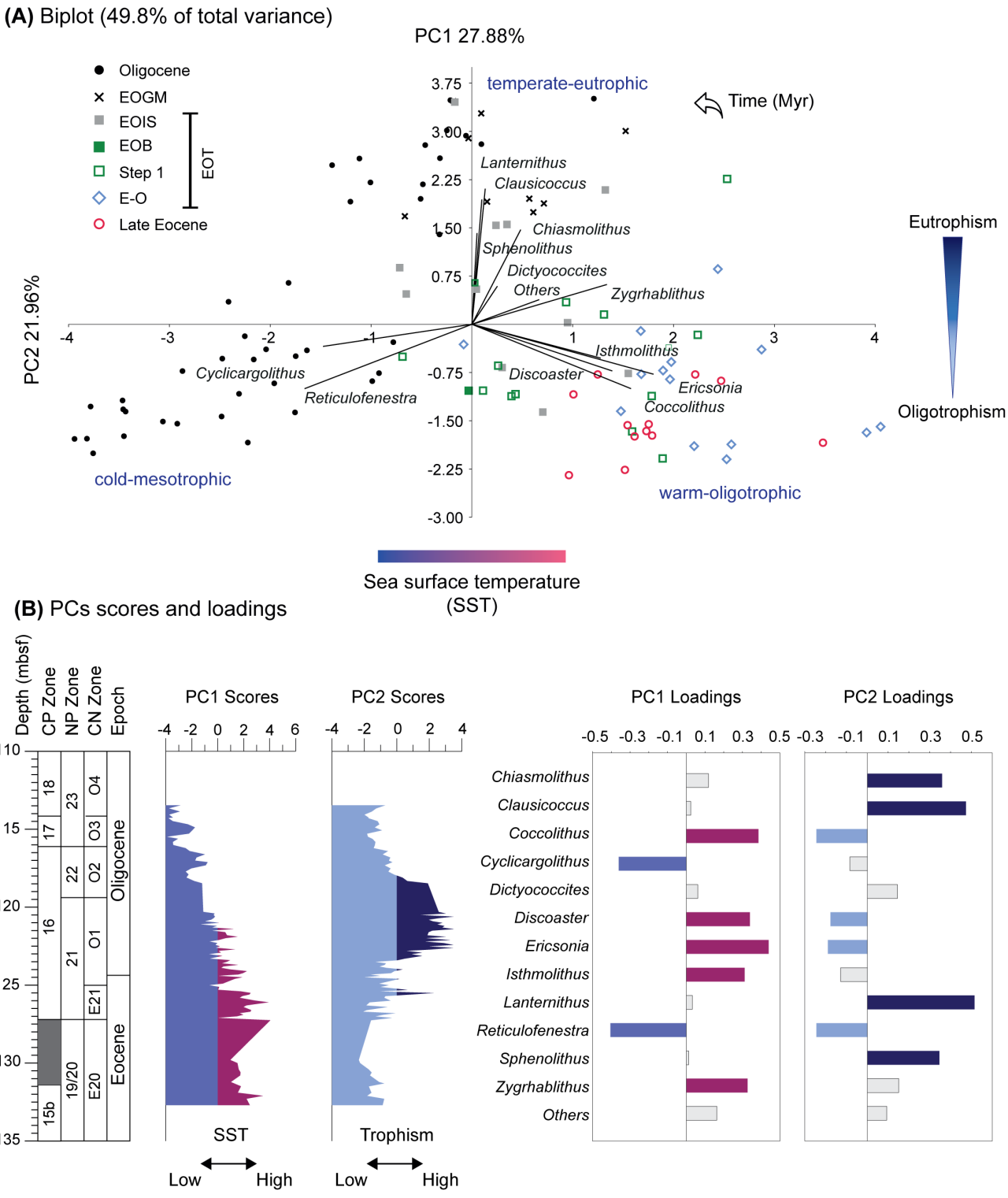
(A) Biplot (49.8% of total variance)
PC1 27.88%
PC2 21.96%
Oligocene
EOGM
EOIS
EOB
Step 1
E-O
Late Eocene
EOT
temperate-eutrophic
Time (Myr)
Lanternithus
Clausicoccus
Chiasmolithus
Sphenolithus
Dictyococcites
Others
Zygrhablithus
Isthmolithus
Discoaster
Ericsonia
Coccolithus
Cyclicargolithus
Reticulofenestra
Eutrophism
Oligotrophism
cold-mesotrophic
warm-oligotrophic
Sea surface temperature (SST)
(B) PCs scores and loadings
Depth (mbsf)
CP Zone
NP Zone
CN Zone
Epoch
PC1 Scores
PC2 Scores
PC1 Loadings
PC2 Loadings
SST
Trophism
Low
High
Low
High

Figure 9

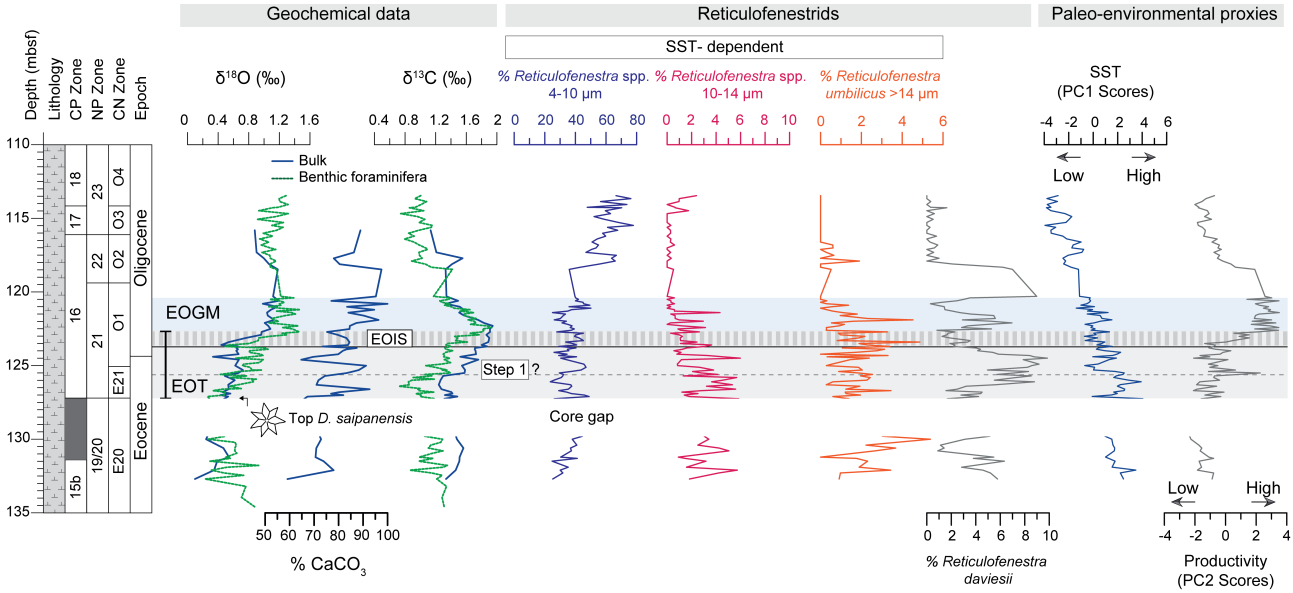
Geochemical data
Reticulofenestrids
Paleo-environmental proxies
SST- dependent
Depth (mbsf)
Lithology
CP Zone
NP Zone
CN Zone
Epoch
δ18O (‰)
δ13C (‰)
% Reticulofenestra spp. 4-10 µm
% Reticulofenestra spp. 10-14 µm
% Reticulofenestra umbilicus >14 µm
SST (PC1 Scores)
Low
High
Bulk
Benthic foraminifera
EOGM
EOIS
EOT
Step 1 ?
Top D. saipanensis
Core gap
Oligocene
Eocene
% CaCO3
% Reticulofenestra daviesii
Productivity (PC2 Scores)

1493 Plate 1

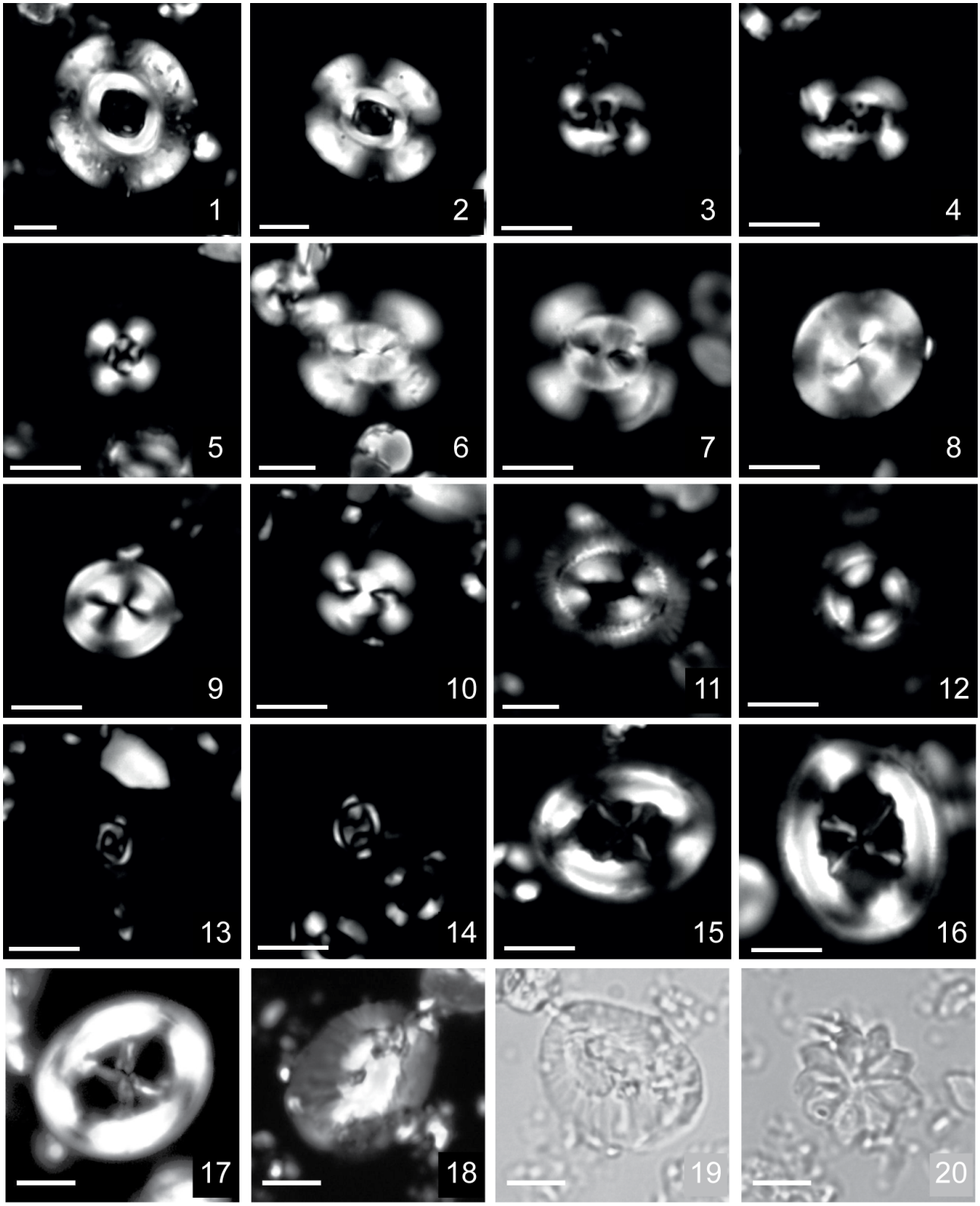

1494

1495

1496

1497

1498

Plate 2

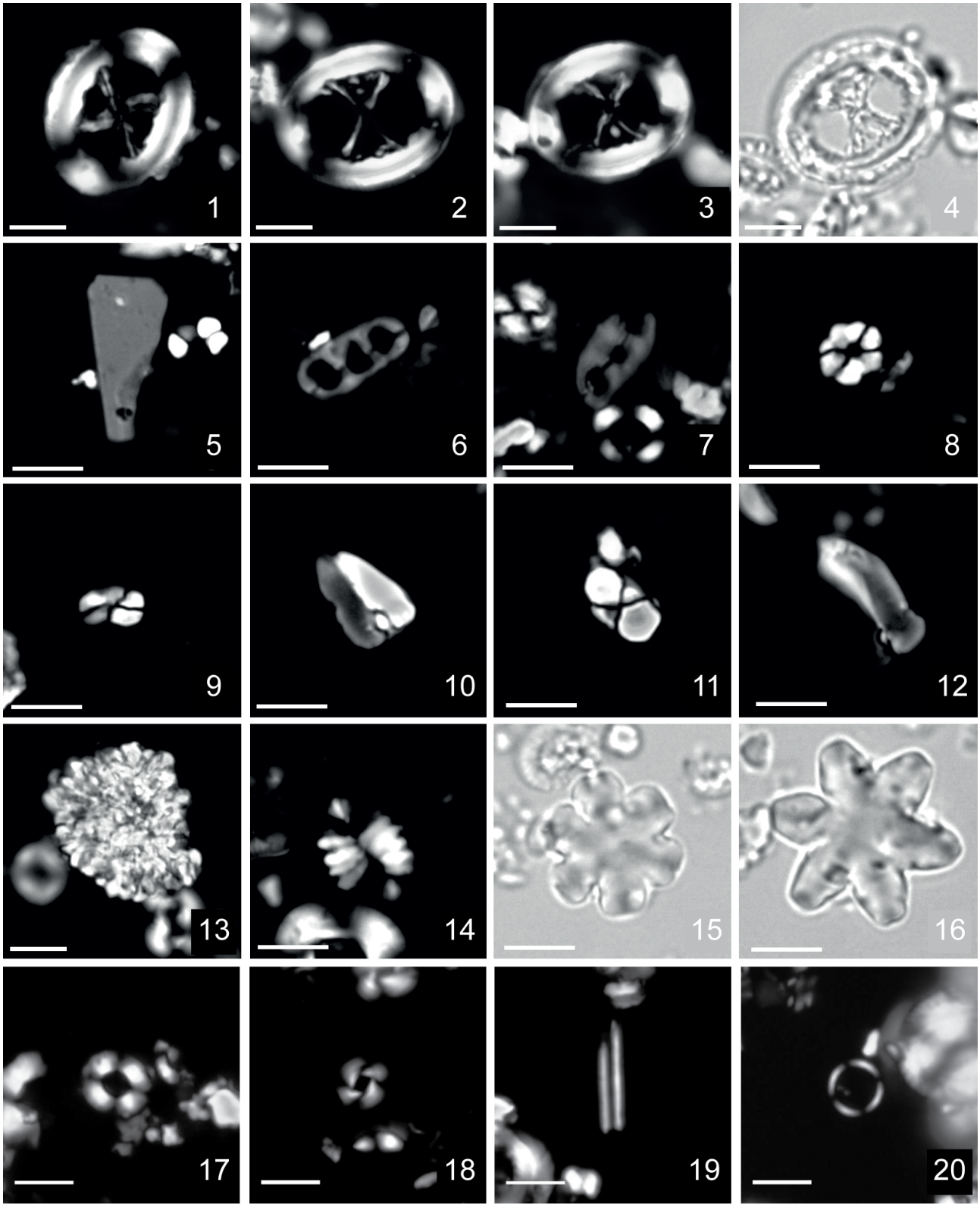

Plate 3

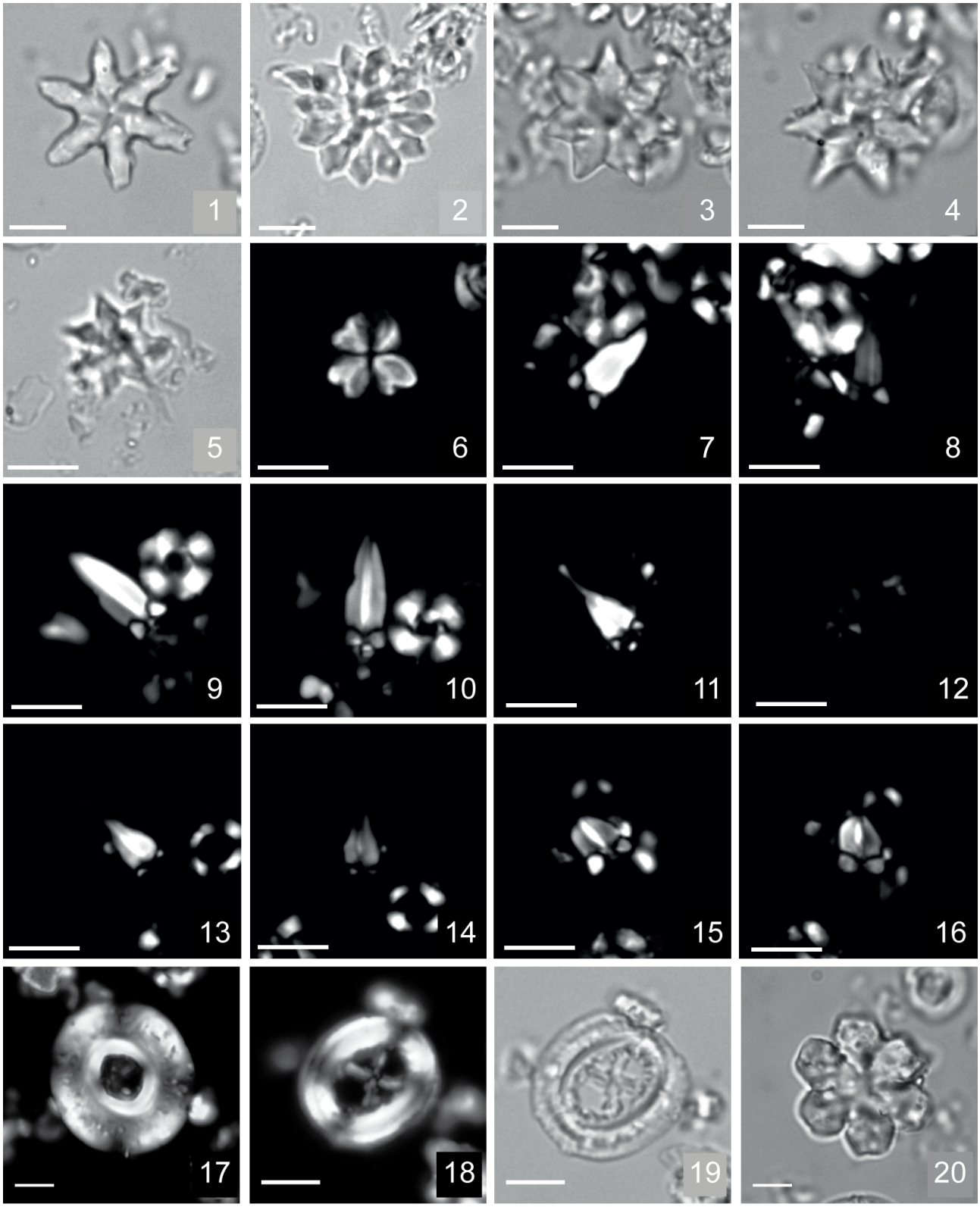

Plate 4